Author Manuscript

Author Manuscript

Author Manuscript

Author Manuscript

HHS Public Access

Author manuscript

Neuroimage. Author manuscript; available in PMC 2023 April 15.

Published in final edited form as:

Neuroimage. 2022 April 15; 250: 118923. doi:10.1016/j.neuroimage.2022.118923.

Hemodynamic and metabolic correspondence of resting-state voxel-based physiological metrics in healthy adults

Shengwen Deng[a,b],

Crystal G. Franklin[a],

Michael O'Boyle[a],

Wei Zhang[a],

Betty L. Heyl[a],

Paul A. Jerabek[a],

Hanzhang Lu[c,d,e],

Peter T. Fox[a,f,g,h,*]

[a] Research Imaging Institute, University of Texas Health Science Center at San Antonio, 7703 Floyd Curl Drive, San Antonio, TX 78229, USA

[b] Department of Radiology, University Hospitals Cleveland Medical Center, Cleveland, OH, USA

[c] The Russell H. Morgan Department of Radiology & Radiological Science, Johns Hopkins University School of Medicine, Baltimore, MD, USA

[d] Department of Biomedical Engineering, Johns Hopkins University School of Medicine, Baltimore, MD, USA

[e] F.M. Kirby Research Center for Functional Brain Imaging, Kennedy Krieger Research Institute, Baltimore, MD, USA

[f] Glenn Biggs Institute for Alzheimer's & Neurodegenerative Disorders, University of Texas Health Science Center at San Antonio, San Antonio, TX, USA

[g] Department of Radiology, University of Texas Health Science Center at San Antonio, San Antonio, TX, USA

[h] South Texas Veterans Health Care System, San Antonio, TX, USA

Abstract

This is an open access article under the CC BY-NC-ND license (http://creativecommons.org/licenses/by-nc-nd/4.0/)

* Corresponding author at: Research Imaging Institute, University of Texas Health Science Center at San Antonio, 7703 Floyd Curl Drive, San Antonio, TX 78229, USA. fox@uthscsa.edu (P.T. Fox).

Author contributions

Fox, Deng and Franklin had full access to all the data in the study and take responsibility for the integrity of the data and the accuracy of the data analysis. *Concept and design:* Fox, Lu, Deng. *Acquisition, analysis, or interpretation of data:* Deng, Fox, Franklin, O'Boyle, Zhang, Heyl, Jerabek. *Drafting of manuscript:* Fox and Deng. *Critical revision of the manuscript for important intellectual content:* Deng, Fox and Franklin. *Statistical analysis:* Franklin and Deng. *Obtained funding:* Fox and Lu. *Administrative, technical, or material support:* Heyl, Jerabek, O'Boyle and Deng. *Study Supervision:* Fox, Lu and Jerabek.

Supplementary materials

Supplementary material associated with this article can be found, in the online version, at doi:10.1016/j.neuroimage.2022.118923.

Author Manuscript Author Manuscript Author Manuscript Author Manuscript

Voxel-based physiological (VBP) variables derived from blood oxygen level dependent (BOLD) fMRI time-course variations include: amplitude of low frequency fluctuations (ALFF), fractional amplitude of low frequency fluctuations (fALFF) and regional homogeneity (ReHo). Although these BOLD-derived variables can detect between-group (e.g. disease vs control) spatial pattern differences, physiological interpretations are not well established. The primary objective of this study was to quantify spatial correspondences between BOLD VBP variables and PET measurements of cerebral metabolic rate and hemodynamics, being well-validated physiological standards. To this end, quantitative, whole-brain PET images of metabolic rate of glucose (MRGlu; ^{18}FDG) and oxygen (MRO_2; ^{15}OO), blood flow (BF; $H_2{}^{15}O$) and blood volume (BV; $C^{15}O$) were obtained in 16 healthy controls. In the same subjects, BOLD time-courses were obtained for computation of ALFF, fALFF and ReHo images. PET variables were compared pair-wise with BOLD variables. In group-averaged, across-region analyses, ALFF corresponded significantly only with BV ($R = 0.64$; $p < 0.0001$). fALFF corresponded most strongly with MRGlu ($R = 0.79$; $p < 0.0001$), but also significantly ($p < 0.0001$) with MRO_2 ($R = 0.68$), BF ($R = 0.68$) and BV ($R = 0.68$). ReHo performed similarly to fALFF, with significant strong correspondence ($p < 0.0001$) with MRGlu ($R = 0.78$), MRO_2 ($R = 0.54$), and, but less strongly with BF ($R = 0.50$) and BV ($R = 0.50$). Mutual information analyses further clarified these physiological interpretations. When conditioned by BV, ALFF retained no significant MRGlu, MRO_2 or BF information. When conditioned by MRGlu, fALFF and ReHo retained no significant MRO_2, BF or BV information. Of concern, however, the strength of PET-BOLD correspondences varied markedly by brain region, which calls for future investigation on physiological interpretations at a regional and per-subject basis.

Keywords

Voxel-Based Physiology; Metabolism; Brain; Hemodynamics; PET; fMRI; BOLD; ALFF; fALFF; ReHo; VBP

1. Introduction

Voxel-wise measurements of the blood oxygenation level dependent (BOLD) signal in the resting state are widely used and have demonstrated regional abnormalities in multiple neurologic (Han et al., 2011; Hou et al., 2014; Li et al., 2002, 2014), psychiatric (Bing et al., 2013; Gray et al., 2020), and developmental disorders (Cortese et al., 2021; Lau et al., 2019). The rapid adoption of these metrics is attributable to several properties that make them highly amenable to clinical application, as follows. Being MRI-based, they can be performed without radiotracers. Measured in the resting state, they require no task-paradigm training and minimize in-scanner compliance, thereby facilitating application in clinical and developmental populations (Cole et al., 2010). With short (12–16 min) acquisitions, analysis pipelines can be performed reliably (Birn et al., 2013) using semi-automated toolboxes such as BRANT (https://sphinx-doc-brant.readthedocs.io/), CONN (https://web.conntoolbox.org/) and DPARSF (rfmri.org/). These voxel-based metrics and coordinate-based reporting can be further used for cross-study meta-analytic comparisons (Sha et al., 2018; Zang et al., 2015), providing statistically valid generalizations of disease patterns (Fox et al., 2014). A notable shortcoming of these methods, however, is that their physiological interpretations

Author Manuscript Author Manuscript Author Manuscript Author Manuscript

are problematic, with a paucity of studies testing their correspondence to traditional hemodynamic and metabolic physiological variables.

The low-frequency band of the BOLD signals is considered reflective of neuronal activity (Biswal et al., 1995), which exhibits periodicity at rest (Golanov et al., 1994). Physiological models demonstrate that the BOLD signal responses are convolved functions of blood volume, blood flow, and utilization rates of oxygen and glucose (Buxton et al., 1998; Heeger and Ress, 2002; Raichle, 1998). Neuronal-modulated hemodynamic fluctuation in BOLD signals can be mostly separated from non-neuronal systemic fluctuations due to cardiac and respiratory cycles by applying low-frequency-band-pass filters (0.01–0.1 Hz, or 0.01 – 0.08 Hz) (Birn et al., 2006; Bumstead et al., 2017; Cordes et al., 2000; Frederick et al., 2012; Magri et al., 2012), although not entirely (Birn et al., 2006; Shmueli et al., 2007; Xifra-Porxas et al., 2021). To quantify dynamics of neuronally modulated BOLD fluctuations, several voxel-based metrics were developed, including fluctuation amplitude (Zang et al., 2007; Zou et al., 2008), fluctuation coherence among neighboring voxels (Zang et al., 2004), and others (Garrett et al., 2013a; Salvador et al., 2007; Tomasi and Volkow, 2010a; Wink et al., 2006). Amplitude of low frequency fluctuations (ALFF) models the amplitude of a specific frequency band (usually 0.01–0.1 Hz) of BOLD oscillations. Fractional ALFF (fALFF) normalizes ALFF with the amplitude of the entire frequency spectrum to reflect the relative contribution of low-frequency fluctuations to the entire pattern (Zou et al., 2008). Regional homogeneity (ReHo) estimates local synchronization of band-filtered BOLD signal among neighboring voxels and, thereby, indicates a co-varying cluster of voxels (Zang et al., 2004). As voxel-based metrics of the BOLD signal, ALFF, fALFF and ReHo are considered to be reflective of local brain properties - independent of long-range connectivity- in spatially discrete regions (Li et al., 2012a,b; Lv et al., 2018). However, the pattern of associations and causal links between these voxel-based BOLD metrics and more traditional voxel-based physiological variables are not well characterized. This shortcoming impedes the physiological interpretation of voxel-wise rsfMRI findings, particularly in the context of neurological and psychiatric disorders and aging-related processes (Gauthier et al., 2013; Girouard and Iadecola, 2006).

Physiological inferences of voxel-based BOLD metrics can be augmented by using a multi-modality, quantitative imaging approach, an endeavor which has been applied in several reports. Arterial Spin labeling MRI and ^{18}F fluorodeoxyglucose (^{18}FDG) positron emission tomography (PET), in conjunction with rsfMRI, have shown that hemodynamics and metabolism are closely associated with BOLD-based metrics (Aiello et al., 2015; Bernier et al., 2017; Fan et al., 2019; Li et al., 2012a,b; Zhang et al., 2018a). Notably, the relative metabolic correspondences of ALFF, fALFF and ReHo are not well established. We would argue that because of the intrinsic complexity of hemodynamic and metabolic influences on the BOLD signal, a comprehensive physiological battery is needed to disentangle the respective contributions of these physiological variables to voxel-based BOLD metrics. Further, the functional architecture of the brain also influences hemodynamic-metabolic coupling, necessitating that optimal interpretation of the BOLD-PET interplay must take these network-based regional variations into account (Di et al., 2019; Di and Biswal, 2012, 2017; Mueller et al., 2013; Taylor et al., 2012; Wehrl et al., 2013; Xu et al., 2019).

Author Manuscript Author Manuscript Author Manuscript Author Manuscript

As hemodynamics and metabolism exhibit strong coupling in the resting state (Hillman, 2014), constancy of local blood supply is most likely regulated to meet the demand of oxidative phosphorylation of glucose (Fox and Raichle, 1986; Lenz et al., 1998, 1999; Roy and Sherrington, 1890), which entails delivery of oxygen and glucose, and removal of metabolic byproducts. ALFF, fALFF and ReHo – although they are hemodynamically derived measures – likely will be mostly driven by, or covary with, baseline metabolic demand, as quantified by metabolic rate of glucose (MRGlu) and metabolic rate of oxygen (MRO_2). Recent reports, using information theory metrics to quantify causality and non-linear relationships in functional neuroimaging, show that blood volume (BV) and MRO_2 have predominant driving influences on blood flow (BF) in neonatal brain (Nourhashemi, 2020; Nourhashemi et al., 2017). This inferential strategy has also been used to quantify causal relationships of voxel-based BOLD metrics and traditional voxel-based physiology, by implementing conditional and interaction analyses with information theory metrics (Rosas et al., 2019), an approach emulated here.

The current study sought: (1) to inform physiological interpretations of widely-used BOLD-based rsfMRI metrics (ALFF, fALFF and ReHo); and, (2) to test the coupling hypothesis of ALFF/fALFF/ReHo with MRGlu and MRO_2. To this end, resting-state measures with two functional imaging modalities were employed: PET and fMRI. PET was used to measure glucose consumption (metabolic rate of glucose, MRGlu), oxygen consumption (metabolic rate of oxygen, MRO_2) and hemodynamics (cerebral blood volume, BV; cerebral blood flow, BF). T2* BOLD was used for a variety of VBP fMRI measurements. Linear associations between voxel-based BOLD metrics, metabolic and hemodynamic physiological variables were identified in across-region and across-subject comparisons. Further, physiological information underlying the voxel-based BOLD metrics was quantified via mutual information and conditional mutual information analyses.

2. Methods

The study protocol was approved by the Institutional Review Board of The University of Texas Health Science Center at San Antonio (HSC20170187H). The radioactive contrast agents used were approved by the institutional Radioactive Drug Research Committee, and an Investigational New Drug Application (IND number: 039789).

2.1. Participants

Study participation was limited to young, healthy controls. Exclusion criteria determined by medical history were: systemic disorders (e.g., diabetes, hypertension), neurological or psychiatric disorders, metal implants, claustrophobia, and pregnancy. Non-pregnancy was confirmed by pregnancy test prior to study enrollment. Sixteen participants (8 males, M, and 8 females, F, 27.5±5.0 years old) were recruited.

2.2. Study procedures

Each subject received MR and PET acquisition on the same day. The MR and PET scanners are physically adjacent (< 1 min walk). For each subject, the MR session included: structural MRI and resting-state fMRI. The PET scan session included: arterial

Author Manuscript Author Manuscript Author Manuscript Author Manuscript

and venous catheterization, transmission scan, two three-tracer ^{15}O tracer sessions and one ^{18}FDG session. All 16 subjects completed the first ^{15}O PET session. Ten subjects (5M/5F, 26.1±4.3 years old) completed both first and second ^{15}O PET sessions. (From this cohort, demographics and test-retest reliability have been previously reported (Jiang, 2020)). Eleven 11 subjects (4M/7F, 26.5 ±4.7 years old) completed the ^{18}FDG session. Fifteen subjects (7M/8F, 26.2 ± 4.4 years old) completed the rsfMRI session.

Plasma glucose, hematocrit were measured from venous blood samples obtained before the PET session. Urinary human chorionic go nadotropin was obtained from women participants. Arterial oxygenation saturation (Ya) was measured using a pulse oximeter during the MR session. All data were de-identified.

2.3. MRI Acquisitions

All MRI experiments were performed on a Siemens 3T system (Trio, Siemens Healthcare, Erlangen, Germany), with a transmitting body coil and a 12-channel receiving head coil. Foam padding was placed to minimize intra-scanning head motion.

Each subject first underwent an anatomical scan using a T1-weighted Magnetization-Prepared-RApid-Gradient-Echo (MPRAGE) sequence, with the following parameters: sagittal slice, voxel size = 1.0 mm isotropic; TR/TE/TI = 2100/4.2/1100 ms; Matrix = 256 (readout direction) × 224 (phase-encoding direction) × 176 (slices); echospacing = 9.4 ms; scan duration = 4.3 min.

Resting-state fMRI was performed using a multiband T2*-weighted gradient echo EPI sequences (Xu et al., 2013), with the following parameters: multi band factor =3; voxel size = 2.4 mm isotropic; TR/TE = 1400/30 ms; Matrix = 88 × 88 × 60 (slices); flip angle = 52°; 700 volumes; scan duration = 16 min. Before the scan began, subjects were instructed to stay still and awake with eyes closed, similar to the resting condition in the PET session. Before the rsfMRI acquisition, subjects were again reminded not to move any part of their body and to keep their eyes closed.

2.4. PET acquisitions

The PET data were acquired on a CTI ECAT HR+ scanner (Siemens, Knoxville, TN). A thermoplastic facial mask was used to minimize head motion during scans. The ^{15}O-labeled tracers were produced by an onsite cyclotron (MC-17, Scanditronix Magnet AB, Sweden).

Before the PET scans, an catheter was placed in a radial artery; an antecubital venous catheter was placed in the contralateral forearm. A transmission scan was performed for attenuation correction.

Subsequently, two sessions of ^{15}O PET scans were performed to sequentially quantify PET-based BV, BF and MRO_2, with different radiotracers ($C^{15}O$, $H_2{}^{15}O$, and $^{15}O_2$). Acquisition parameters details for ^{15}O PET have been described in (Jiang et al., 2021).

For the ^{18}FDG scans, after bolus intravenous administration of 5mCi±10% FDG, 70 frames of 3D dynamic emission scans were acquired over 70 min (70 frames x 1 min). Sixteen

Author Manuscript Author Manuscript Author Manuscript Author Manuscript

arterial blood samples (about 1.5 mL each) were collected to calculate the arterial input function (6 × 30s, 10 × 10min). After centrifuge, blood serum was extracted to determine the arterial input function.

During scans and arterial blood sample acquisition, subjects laid quietly in a dark room with their eyes closed. PET reconstruction was by filtered back-projection using a 3 mm smoothing kernel, resulting in a voxel size of 2.0 × 2.0 × 2.4 (slice) mm^3.

2.5. RsfMRI data processing

Calculation of ALFF, fALFF and ReHo was performed in Matlab (Mathworks Inc.) using DPARSF (V5.1, http://rfmri.org/DPARSF) (Yan and Zang, 2010). The first 10 time points were deleted. The EPI images were slice-timing corrected and realigned. Subsequently, EPI images were regressed for nuisance covariates that were unrelated to neuronal activity (white matter, CSF, and head motion). Nuisance regression used Friston 24-parameter model for head motion (Friston, 1996). For white matter, and CSF, the mean timeseries across voxels were regressed out, using DPARSF default recommended parameters. To eliminate the effects of spatial smoothing on the indices, the original voxel size (2.4mm) was used in the spatial normalization using DARTEL (Ashburner, 2007).

ALFF/fALFF were calculated with filtered signals within the low-frequency range (0.01–0.08 Hz) without additional filtering. Specifically, fractional ALFF was computed by the ratio of the filtered frequency band (0.01 – 0.08 Hz) against the whole-available frequency band (limited by the imaging acquisition). ReHo was computed via Kendall's coefficient of concordance (KCC) as a local coherence metric of BOLD signal (Zang et al., 2007), with 27 neighboring voxels without smoothing.

All parametric images were calculated in native space and then normalized to the 2 mm Montreal Neurological Institute (MNI) template (Fonov et al., 2009).

To validate the reliability of the resting state scan, the 16 min time series were split into half samples (350 volumes per half-sample) and the same analyses as the whole time series (700 volumes) were performed. Inter-class correlations were computed to quantify the reliability of BOLD metrics between the two split datasets and between the first 350 volume versus the whole 700 volume dataset. Additionally, framewise displacement of the 16 min scan was calculated to indicate the quality of resting state acquisition, using FSL. Together, resting state fMRI reliability was quantified with framewise displacement during acquisition and voxel-wise inter-class correlation (ICC) of BOLD metrics, applying the gray matter mask from MNI ICBM 152 template. Generally, ICC >0.75 was considered of excellent agreement.

To simplify cross-subject comparisons, various normalization methods were applied to the rsfMRI metrics. ALFF/fALFF/ReHo was transformed into Z-scores by subtracting mean values within the gray matter mask, and then dividing by the standard variation within the mask. Two types of reported normalized rsfMRI metrics (z-normalized, and demeaned, with a MNI gray matter and white matter mask) were also provided for further analyses, as normalized ALFF/fALFF/ReHo is commonly used in the literature. These two types of

Author Manuscript Author Manuscript Author Manuscript Author Manuscript

normalized maps (z-normalized and demeaned) were primarily used in visualizing spatial similarities between rsfMRI metrics and PET hemodynamic-metabolic metrics, and inter-subject comparisons.

2.6. PET data processing

Modeling was performed per subject using the Raichle method for BF (Raichle et al., 1983) and BV (Grubb et al., 1978)), the Mintun method for MRO_2 (Mintun et al., 1984), and the Phelps method for MRGlu (Phelps et al., 1979) with blood volume correction threshold of 8 ml/100g. The brain tissue density was assumed to be 1.05 g/ml. The small vessel to large vessel hematocrit ratio was assumed to be 0.85 (Grubb et al., 1973). For robust BV and MRO_2 estimation, minimal delay and dispersion correction were performed, in accordance with other studies (Cho et al., 2020). Other details for ^{15}O PET scans and processing are described in a previous publication (Jiang et al., 2021).

Dynamic ^{18}FDG raw data were corrected for potential motion using rigid-body (6 DOF) registration between each frame and the mean images using FLIRT in FSL (Jenkinson, 2001), with a mutual information cost function. Signals in the last 40 min were used for kinetic analyses using the Schimidt model (Schmidt et al., 1992). For static MRGlu, the lumped constant was set to 0.52. Effects of blood volume in BF and MRO_2 were corrected in the modeling methods. The effect of blood volume in MRGlu was corrected using the BV map as weights. Venous vasculature in the BV map was masked using a threshold of 8 mL/100 g and further manual inspection.

Parametric maps of BF, MRO_2 and MRGlu were linearly registered to individual T1w brain images with FLIRT, and then non-linearly normalized to 2mm MNI ICBM space using FNIRT in FSL (Jenkinson et al., 2002; Jenkinson and Smith, 2001), with a mutual information cost function. BV maps were normalized with the deformation maps generated during spatial normalization of BF maps. Per findings in related reports, partial volume effects cause minimal overestimation of the correlations between FDG/MRGlu and ALFF/ReHo (Jiao et al., 2019). Head motion during dynamic scans may introduce errors during partial volume correction, especially when signal-to-noise ratio is low (Bettinardi et al., 2014). Partial volume effect correction in raw data was not performed, except for BF using the Iida method (Iida, 1988; Iida et al., 1991). To minimize partial volume effects in regional analysis, no additional smoothing was applied beyond registration and spatial normalization, as suggested in recent metabolism-flow-coupling reports (Cho et al., 2020; Fan, 2020; Henriksen et al., 2021; Hyder, 2016; Ishii, 2020; Narciso, 2021; Wesolowski et al., 2019). A threshold of BV (>10) was chosen to exclude any voxels that are likely to be in the large vein ventricles.

2.7. Statistical analyses

2.7.1. Spatial similarity—Spatial similarity between the z-normalized metrics was performed with voxel-wise paired T-test in each pair, to identify regions with significantly different regional contrasts between the modalities. Multiple comparison correction was performed with the Threshold Free Cluster Enhancement algorithm in PALM (Winkler et al., 2014) (family wise estimation corrected p threshold of 0.05, 5000 permutations), as null

Author Manuscript Author Manuscript Author Manuscript Author Manuscript

models for multi-modality brain imaging are still being actively develped (Alexander-Bloch et al., 2018; Markello and Misic, 2021). Surface views were rendered using BrainNet Viewer (Xia et al., 2013), with a corrected p threshold of 0.01. Voxel-wise spatial cross-correlations across the gray matter and white matter were quantified using fslcc in the FSL toolbox. Due to differences in acquisition protocols, image contrast mechanisms, spatial and temporal resolution, MR measurements of BOLD signal and PET measurement of brain physiology were considered as independent. Per-subject static images were concatenated into a 4D image as input for fslcc.

2.7.2. Across-region correlation—The across-region correlation analysis was performed for each pair of metrics in group averaged images by Pearson's linear correlation, both in a weighted and unweighted manner. Tests of normality were performed before running the linear correlations. Mean values of each metric in standardized space were extracted using AAL-specified regions (116 ROIs for each metric). To avoid potential signals from non-gray-matter tissues, no dilation of ROIs was implemented. Additionally, to inform the effect of gray matter/white matter contribution to the correlation of values, partial correlations regressing out gray matter and white matter probability were performed in a voxel wise manner (details in Supplementary Result 1.2 Table D). As all images were normalized to the MNI 2 mm template, gray matter (GM) and white matter (WM) probability were estimated with the gray matter and white matter partial volume maps of the MNI template, using FSL FAST. This partial correlation approach was performed on a voxel-wise basis rather than on a ROI basis. The reason for this is that the value distribution of GM/WM probability within AAL ROIs were heavily tailed and had many extreme values (0 and 1), with the ROI-mean value of GM/WM probability not truly representing the probability of GM/WM. Consequentially, the resulting mean values of ROIs in the GM/WM probability map did not truly represent overall GM/WM partial volume effect within a ROI. To further clean potential signals from white matter and CSF, a group-averaged gray matter probability mask, generated by DARTEL segmentation, was applied prior to choosing the respective ROIs. Before the calculation of correlation, ROI values outside of 25%–75% quantiles were considered as outliers and removed in the subsequent analyses. A one-sample t-test was performed on correlation coefficients using Matlab, to test against the null hypothesis that the mean correlation coefficient was zero. For multiple comparison correction, a threshold of $P < 0.0001$ was utilized, (Bonferroni correction $p = 0.05/116 = 0.00043$).

2.7.3. Mutual information—Mutual information (MI) and other information theoretic quantities were calculated with the GCMI toolbox in (https://github.com/robince/gcmi). Conceptually, the entropy of each metric in group-averaged maps was quantified in bits with bias correction (Ince et al., 2017a). Conventional MI and Gaussian-Copula Mutual Information (MI normalized with Gaussian-Copula) were computed for each pair of metrics. To investigate interaction and synergy properties, conditional GCMI was calculated for each rsfMRI metric with various pairs of BF, BV, MRO_2 and MRGlu. The term "condition" indicated how much MI is shared within two primary variables given the MI of the conditional variable is removed. Interaction Information (II) was calculated by subtracting MI with conditional MI to compare coupling or synergistic characters in different rsfMRI-

Author Manuscript Author Manuscript Author Manuscript Author Manuscript

PET combinations, with the high II indicating synergistic and low II indicating coupling tendency. Theoretically, conditional MI is non-negative, while II can be positive, zero, or negative.

3. Results

Fig. 1 illustrates the acquisition and processing pipeline of the dataset. Mean values in gray matter, white matter and gray matter + white matter are reported (Supplementary Results 1.1 Table A). As this paper focuses on group-level physiological interpretation of BOLD metrics, PET-data reliability was quantified with inter-subject coefficient of variation (Supplementary Results 1.1 Table A).

For head-motion during rsfMRI acquisition, mean framewise displacement of the whole imaging series across subjects was 0.22 ± 0.06 mm. This was consistent with the framewise displacement in first half of time-series (0.21 ± 0.05 mm) and in the second half (0.23 ± 0.06 mm).

As for reproducibility of BOLD metrics, inter-class correlation of BOLD metrics computed from the split dataset were all larger than 0.75 (ALFF: 0.86 ± 0.16, fALFF: 0.88 ± 0.16, ReHo: 0.84 ± 0.15). Inter-class correlation between the first dataset (340 volumes) and the whole-time-series dataset (700 volumes) were larger than 0.75 as well (ALFF: 0.88 ± 0.16, fALFF: 0.88 ± 0.16, ReHo: 0.91 ± 0.16. Additionally, for BOLD-PET associations, the two subsets of data were similar to the whole dataset in across region correlation analyses (Supplementary Results 1.1 Table B).

Fig. 2 illustrates spatial similarities between voxel-based BOLD matrices and the PET hemodynamic-metabolic battery in z-normalized values, (original values are compared in Supplementary Fig. 1). To quantify the spatial similarity, spatial cross-correlations between BOLD and PET metrics were reported on group-averaged level (Table 1, A). Paired T-test (Fig. 3) identified regions of different values between the z-normalized maps. The pattern identified by voxel-wise T-test agreed with the voxel-wise cross correlation results (Table 1, upper), as follows. Spatial contrast (i.e. z-normalized value) of ALFF was similar to BV, with few voxels identified as significantly different in Fig. 3a. Like-wise, spatial contrast of fALFF and ReHo were not different from BF and MRO2 (Fig. 3f, 3g, 3j, 3k). Although fALFF and ReHo had the highest voxel-wise spatial cross correlation with MRGlu, there were specific regions that the z-normalized values of fALFF and ReHo did not agree with z-normalized MRGlu (Fig. 3h, 3i). The detailed layout of these surface-projected maps is provided in the Supplementary Materials 2.2, 2.3 and 2.4.

Across-region correlation confirmed the metabolic correspondence of fALFF and ReHo values. fALFF and ReHo were highly correlated to MRGlu and MRO_2; ALFF was correlated to BV. This pattern was quantified in group-level, across-voxel correlations, as follows (Fig. 4, Table 1, lower). ALFF and fALFF were correlated with BV ($r = 0.64$, 0.68; $p < 0.0001$); fALFF and ReHo were significantly correlated with BF ($r = 0.68$, 0.50), MRO_2 ($r = 0.68$, 0.54) and MRGlu ($r = 0.79$, 0.78, highest) ($p < 0.0001$). ALFF, though correlated with ReHo and fALFF, did not show strong significant correlations with

Author Manuscript Author Manuscript Author Manuscript Author Manuscript

BF, MRO_2, and MRGlu. For PET measurements, strong correlations of MRGlu-MRO_2 and BF-MRO_2 were identified in the current dataset (Supplementary Results 1.2 Table A). Spearman partial correlation, regressing out partial volume contribution of gray matter and white matter on a voxel wise basis, showed results in good agreement with the across-region results (Supplementary Results 1.2 Table D). ROI-based partial volume correction was not performed in the ROI-based analyses (illustrated in Methods 2.7 Statistical analyses).

Pearson correlations weighted for the size of the ROIs (AAL template), indicated the same pattern of association, with slightly higher correlation coefficients in BF, MRO_2, and MRGlu (Supplementary 2.5 Fig. 5). Specifically, the correlation of BV versus ALFF/fALFF/ReHo was not likely to be affected by weights. Mutual information indices (MI and GCMI) across voxels further verified the association pattern, suggesting that fALFF and ReHo contained information from blood flow, oxygen, and glucose utilization. As GCMI is a normalized form of conventional Mutual Information (Ince et al., 2017a), GCMI was generally lower in values than MI.

To further investigate whether the above-reported BOLD-metabolic correspondence is consistent in per-subject findings, voxel-wise cross correlation and region-wise linear correlation across modalities were also reported in Table 1 c and d. Overall, the degree of correlation is consistent (i.e. small standard deviation of the correlation coefficient), but the strength of correlation is weak (i.e. the p value is larger, and the correlation coefficient is smaller). Only ReHo showed a similar significant association with MRGlu ($p < 0.0001$ after Bonferroni correction), while fALFF and ALFF showed non-significant weaker correlations with respective metrics. Additionally, the respective metabolic and hemodynamic correspondence of both z-normalized and demeaned BOLD metrics were provided in Supplementary Result 1.2 Table B and C, as these results were in good agreement with the major findings to be reported in the manuscript.

Using AAL regions sampled within the brain, conditional MI further characterized the coupled and non-coupled physiological association of rsfMRI metrics (Fig. 5). Fractional ALFF and ReHo still contained information from oxygen and glucose consumption, when neglecting the contribution of BF (Fig. 5 c, with BF as a condition, conditional MI all > 0.1 bits). On the other hand, BF-specific information was minimal when neglecting the contributions of oxygen or glucose consumption (Fig. 5 d and e, with MRO_2 and MRGlu as conditions, conditional MI all < 0.03 bits). There was limited MRO_2 information when neglecting the contribution of BF. This discrepancy indicates that the BF information in fALFF/ReHo was highly metabolically coupled. When neglecting MRO_2-specific information, MRGlu specific information remained in the fALFF and ReHo signal (conditional MI = 0.24, 0.41 bits, respectively). After removing the MRGlu-specific information, minimal BF and MRO_2 information remained in the fALFF and ReHo signal (Fig. 5 e). Mutual information and conditional mutual information are theoretically nonzero. Interaction information can be either positive, negative or zero, which is reported to be suggestive to causality besides descriptive statistics (Colenbier et al., 2020; Ghassami and Kiyavash, 2017; Nourhashemi et al., 2017; Young et al., 2021).

Author Manuscript Author Manuscript Author Manuscript Author Manuscript

Interaction Information was highest with a combination of fALFF, MRO_2, and MRGlu (likewise for ReHo, MRO_2, and MRGlu), indicating these combined variables are synergistic (Fig. 4 right). Interactions between ReHo/fALFF, BF, and MRO_2 were not as high as interactions between ReHo/fALFF, MRO_2, and MRGlu, indicating that a part of BOLD-metabolic interactions was not likely to be flow coupled. Negative interaction information (Ince et al., 2017a) in ALFF indicated the non-weak association among BF, MRO_2, and MRGlu. Specifically, negative but close to zero (<0.01 bits) values were identified in conditional mutual information analyses. Negative interaction information was identified between ALFF:CBF/MRO2:MRGlu (<-0.01 bits). This indicates that although mutual information ALFF:MRGlu is very close to zero, both ALFF and MRGlu are associated with CBF and MRO2.

4. Discussion

The overarching hypothesis of voxel-based BOLD-metabolic coupling was confirmed for fALFF and ReHo and disconfirmed for ALFF. CMGlu and, to a lesser degree, MRO_2 provided the preponderance of metabolic information for fALFF and ReHo. Blood flow information in fALFF and ReHo were largely metabolically coupled. By contrast, ALFF was most strongly correlated with BV, having little information from MRGlu, MRO_2 or BF. Regional and network-specific inter-subject correlations demonstrated that BV robustly covaried with ALFF, fALFF, and ReHo in frontoparietal and cerebellum networks across subjects. In these robust BOLD-physiology coupled regions, conditional mutual information analyses also identified non-flow-coupled metabolic information in fALFF and ReHo (Supplementary Fig. 2.6). Additionally, the blood flow information contained in fALFF and ReHo was largely metabolic coupled.

A paucity of studies have addressed the hemodynamic-metabolic correspondence of ALFF, fALFF, and ReHo. Li (Li et al., 2012b) and Aiello (Aiello et al., 2015) first reported spatial similarities of ALFF and ReHo versus blood flow and glucose metabolism, respectively, in the resting state brain. These early studies reported across-region correlations of ReHo and FDG uptake to be 0.47–0.73 (Aiello et al., 2015), 0.51–0.83 (Fu et al., 2018) and 0.68 (Bernier et al., 2017) using different temporal-filtering and ROI sampling methods. All of these prior reports are in agreement with coefficients observed in the current data (0.78). As well, significant correlations of fALFF/ReHo, BF/MRO_2, MRO_2/MRGlu, and BF/BV in the current dataset (Supplementary Results 1.2. Table A) indicated the reliability of respective measurements, as such coupling relations at rest have been demonstrated in an extensive literature (fALFF/ReHo (Nugent et al., 2015; Yuan et al., 2013), BF/MRO_2 (Fox and Raichle, 1986), MRO_2/MRGlu (Vaishnavi et al., 2010), and BF/BV (Grandin et al., 2005; Wesolowski, 2019).

For BOLD-hemodynamic association, across-region correlation of voxel-based BOLD metrics and BF, as measured with Arterial Spin Labelling MRI, was reported to be 0.41–0.49 for ALFF (Li et al., 2012b; Zou, 2015), and 0.19–0.28 for ReHo (Li et al., 2012b), while the current data showed a weaker correlation (weighted r (ALFF/BF) = 0.43 Supplementary Fig. 5; r(mALFF/BF) = 0.37, r(mReHo/BF) = 0.50, Supplementary Results 1.2 Table B). Variations of findings in the ALFF/BF association may be due to

Author Manuscript Author Manuscript Author Manuscript Author Manuscript

different normalization methods, accuracy of registration, underlying venous vasculature (Li et al., 2012b; Vigneau-Roy et al., 2014) and proximity to ventricles in ROI samples (Zuo et al., 2010). Also, PET calculation of BF corrects for blood volume contamination via a small-to-large vessel ratio, which limits the contribution of BV in the current ALFF/BF analyses. Indeed, some studies showed that regions with high baseline BF may not have a high fluctuation amplitude (Zou et al., 2009).

Across-voxel correlation of normalized ALFF and MRGlu is not significant in the current study, although reported as significant in other studies (Nugent et al., 2015; Tomasi et al., 2013). One prior study compared regional MRGlu to normalized ALFF and reported nonsignificant correlation in young adults (r = 0.001) (Bernier et al., 2017). Potential explanations for this disagreement are the BV correction in the MRGlu calculation, and the different frequency of filtering in the current study compared with initial reports by Tomasi and Nugent. A recent study by Jiao et al. (2019), which used multiple band-filtering methods including the band used in the current study (0.01 – 0.08 Hz), reported a weak but significant correlation between ALFF/MRGlu (r = 0.198), and moderate correlations between fALFF and ReHo versus MRGlu (r = 0.30, 0.53, respectively), which partly overlap with the current findings.

On the other hand, a significant correlation between ALFF and BV was observed. BV has been considered as a measurement of venous vasculature (Martin et al., 1987) and as a marker of microvascular density (Pathak et al., 2001). Vascular density and oxygenation in venules are found to contribute largely to the amplitude of the BOLD signal at rest, with an across-region correlation of 0.43 (Vigneau-Roy et al., 2014). This is in line with the current findings of ALFF/BV correlation, which shows stronger across-region correlation (r = 0.64, Table 1a; weighted r = 0.70, Supplementary Fig. 2.5). This association is partly concordant with the resting state findings of Kim et al. (1994) and with modeling of neurally induced oxygenation changes described by (Turner, 2002), which found that the amplitude of BOLD signals was greater along draining veins. In highly vascularized voxels, hemodynamic fluctuations, such as vasomotion and oscillation of microcirculation around 0.1 Hz (Mayhew et al., 1996; Razavi et al., 2008), may contribute to the ALFF signal (Vigneau-Roy et al., 2014). This hypothesis may explain findings in patients with glioma, where an increase of ALFF and cerebral blood volume both accompany tumor-induced neovascularization (Emblem et al., 2008; Yang et al., 2021). Also, cortical areas with higher baseline BV show a higher BOLD response at task (Davis, 1998; Vigneau-Roy et al., 2014; Yu et al., 2012).

Mutual information theory (MIT) analyses were used to inform causal inference and interactions regarding voxel-based BOLD metrics and PET hemodynamic, and metabolic metrics. A multi-collinearity relation exists among the voxel-based BOLD metrics, glucose and oxygen utilization, blood volume and blood flow at rest. In this situation, statistical inferences methods, such as partial correlation and general linear modeling, may inflate the variance of regression and mislead inferences regarding relevance (Dormann et al., 2013). Mutual information theory can supplement correlation analyses by quantifying shared information among variables including potential non-linear non-monotonic interdependencies (Song et al., 2012). MIT has been applied to quantify correlations of

Author Manuscript Author Manuscript Author Manuscript Author Manuscript

structural-functional image registration (Maes et al., 1997), neuron oscillatory dynamics (Schyns et al., 2011), and, more recently, functional neuroimaging data (Ince et al., 2017a). Beyond the strength of association, mutual information can estimate coupling/synergy properties between BOLD-based and PET metabolic-hemodynamic metrics, via conditional and interaction analyses (Ince et al., 2017a; Olbrich, 2015). With this measurement, the metabolic information in fALFF and ReHo signal was reconfirmed. This supports the notion that fALFF and ReHo are potentially metabolic proxies (Bernier et al., 2017).

With multi-level conditional MI analyses, the respective contributions of hemodynamic and metabolic metrics were confirmed. After removing the effect of MRGlu or MRO_2, the remaining physiological information in fALFF and ReHo was minimal. This indicates that baseline BF information in fALFF and ReHo is largely attributable to underlying metabolic utilization. Jiang and Zuo (Jiang and Zuo, 2016) hypothesized that regions with high MRGlu showed enhanced ReHo due to enhanced hemodynamics, as higher glucose utilization requires higher perfusion (Huisman, 2012). The statistical inference from mutual information supports this causal inference: the fALFF/ReHo-BF association is likely to reflect inherent BOLD-metabolic coupling. Recent reports, using similar MIT measurements, show that BV and MRO_2 drive baseline BF in neonatal brain in the resting state (Nourhashemi, 2020; Nourhashemi et al., 2017). These information theory findings extended early findings that different metabolic-demand conditions at rest may alter the ratio between low-amplitude BOLD and perfusion fluctuations (Fukunaga et al., 2008).

Also, conditional MI indicated that the metabolic information in voxel-based BOLD metrics was not accompanied by blood flow demand. Glucose, as a fuel of brain, is incorporated into neuronal glutamate (Shen et al., 1999) along with ongoing metabolic activities in neurons (Shen, 2013). Cerebral metabolic rate of glucose consumption is reflective of energy demand during oxidative phosphorylation of glucose, part of which covaries with metabolic rate of oxygen consumption, and glycolysis processes (Huettel et al., 2004; Magistretti et al., 1999; Raichle and Mintun, 2006). Further, glucose consumption is associated with glutamatergic synaptic activity (Shen et al., 1999) and synaptic density (Rocher et al., 2003; Stoessl, 2017). Beyond these associations, MRGlu is highly correlated with gamma-aminobutyric acid A–binding function across the whole brain (Nugent et al., 2015), potentially due to coupled GABA and glutamate activities at rest (Tremblay et al., 2013). Recent *in vivo* studies of glucose utilization and synaptic density further report regional variation of this association, partly because of varying levels of aerobic glycolysis and energy demand of inhibitory/excitatory synapses (van Aalst et al., 2021). Although no direct comparison of fALFF, ReHo versus glutamatergic/GABAergic function has been reported in the literature, there is evidence of an association between synaptic activity and BOLD signal at rest (Ekstrom, 2010). A supporting hypothesis is that synaptic changes will affect MRO_2 (Di and Biswal, 2017). The change in synaptic activity, before and after motor training, is accompanied by baseline changes in MRO_2 and MRGlu, but not in BF (Shannon et al., 2016). Therefore, the BOLD signal has great potential to map longitudinal disease-related synaptic and baseline metabolism changes (Brickman et al., 2009; Small, 2003). A recent report indicated that increased glutamate is accompanied by decreased ReHo in basal ganglia in a subtype of depression, although an exact explanation is lacking

Author Manuscript Author Manuscript Author Manuscript Author Manuscript

(Haroon et al., 2018). Clarification of the association between ReHo and synaptic function requires further experimentation.

In the current study, normalized MRGlu did not agree with zfALFF and zReHo in some brain regions, showing a spatial pattern consistent with another recent report by Wang (Wang, 2021). This replicable regional disagreement superimposed upon a pattern of overall concordance, may be due to the different time-scales of by PET and BOLD MRI, per Wang (Wang, 2021). As an alternative explanation, regional metabolic-balance ($MR0_2$:MRglu) variations may be in play. Although the temporal and regional linkage between neural activity and cerebral blood flow is generally considered consistent at rest (Phillips et al., 2016), metabolic-pathways preferences can differ regionally. Vaishnavi et al., 2010 reported that the MRglu:MRO_2 ratio varied regionally, with some regions (e.g. medial frontal and posterior cingulate) consuming excess glucose. Comparison of BOLD-based metrics with MRglu indicated a similar pattern of (Shokri-Kojori et al., 2019). Interestingly, the same regional pattern was observed in our current data for MRGlu-fALFF/ReHo disagreement, after intensity normalization.

On the other hand, the intensity normalization applied in the current study may also change regional contrast. Although z-normalization is recommended as increasing the inter-subject reliability of BOLD metrics (Yan et al., 2013), intensity normalization may alter image texture (Carré et al., 2020) and disease-related effects (Nugent et al., 2020). Given the prevailing application of intensity normalization in both rsfMRI and PET community, further investigation is needed to determine whether the regional disagreement of normalized BOLD and MRGlu contrast is reflective of regional difference in physiology or a normalization artifact.

Given that low-pass filtering (<0.08 or 0.1 Hz) is commonly used in voxel-wised BOLD metrics analyses as a default pipeline (Yan and Zang, 2010), several studies have reported that BOLD fluctuations at frequencies below 0.1 Hz can share variances with fluctuation in cardiac/respiratory recordings (heart rate and respiratory bellows) (Birn et al., 2006; Chang et al., 2009; Chen et al., 2020; Power et al., 2017; Shmueli et al., 2007; Xifra-Porxas et al., 2021), end-tidal CO2 and arterial CO2 levels (Chang and Glover, 2009b; Lewis et al., 2020; Liu et al., 2017; Prokopiou et al., 2019), and pulse oximetry (Verstynen and Deshpande, 2011). Multiple model-based, data-driven, and hybrid noise-removal strategies are being actively developed (Beckmann et al., 2005; Behzadi et al., 2007; Birn et al., 2008; Chang and Glover, 2009a; Kasper et al., 2017; Kassinopoulos and Mitsis, 2019; Kundu et al., 2012; Power et al., 2017, 2018; Pruim et al., 2015). Although these studies are mostly focusing on inter-regional functional connectivity, non-neuronally-driven physiological confounds on voxel-wise BOLD metrics call for further investigation. Indeed, global signal regression not only has effect on inter-regional BOLD signal correlation (i.e. functional connectivity) (Murphy and Fox, 2017), but also have complex effects on voxel-wise physiological metrics (Qing et al., 2015). As an alternative to global signal regression, nuisance signal regression of motion parameters, mean white-matter and CSF time series was implemented to reduce non-neuronally driven BOLD fluctuations on the current study, in accordance with a pipeline readily available to the neuroimaging community (Yan et al., 2013; Yan and Zang, 2010). Nonetheless, the band-pass filtering and

Author Manuscript Author Manuscript Author Manuscript Author Manuscript

nuisance signal regression applied in the current study did not remove entirely the influence from non-neuronal systemic fluctuations. Of note, the remaining signals, although driven by hemodynamics during respiration bellows, cerebral-vascular reactivity and/or cardiac cycles, also can show regional variability that is spatially similar to specific brain networks (Bright et al., 2020; Chen et al., 2020). Additionally, a recent animal study illustrates regional variability of neurovascular-metabolic coupling between cortical and sub-cortical regions (Shaw et al., 2021). Together, filtered BOLD signals are reported to covary both with local vasculature and systematic hemodynamics, which also are considered to be informative for brain functional architecture. To improve BOLD signal quality and interpretation, more advanced casual inference strategies are needed to better link BOLD-derived metrics with the information underlying neuronal activity (Ekstrom, 2021), as explored in the current mutual information analyses.

4.1. Limitations and future directions

The current study has several limitations, as follows. The first limitation is the potential contribution of signals from large vessels. Previous studies have demonstrated the necessity of removing pixels containing large vessels for BF and BV analyses (Kudo et al., 2003). In the current study, the contribution from the large vessel is corrected via an overall threshold in the BV maps, a small-to-large vessel ratio in the BF calculation, and correction of blood volume signal in MRO_2/MRGlu calculation. Using a lower threshold in the BV map could improve the correlation between BV and fALFF/ReHo, but would also eliminate true gray matter pixels. Indeed, reports which have positive ALFF/ MRGlu, and ALFF/BF correlations did not perform blood volume correction for the FDG and BF data, due to limitations of data acquisition.

Another limitation is the possible effect of partial volume correction. Earlier studies reported a considerable effect of partial volume correction on correlation coefficients (Aiello et al., 2016; Jiao et al., 2019). Specifically, Jiao et al., 2019 reported that partial volume correction on FDG images will lower the coefficient, but not the significance of findings. This result agrees with a quantitative study comparing MRGlu and rsfMRI indices using a static FDG acquisition (Aiello et al., 2016). Indeed, partial volume correction on raw PET data with MR images may influence the accuracy of kinetic modeling and produce spatially different metabolic patterns (Aiello et al., 2016; Andersen et al., 2014; Greve et al., 2016; Hitz et al., 2014). There is limited consensus on optimal correction methods for dynamic PET data (dynamic ^{15}O and ^{18}F data in the current study), largely due to intra-scanning head-motion and low image contrast (Bettinardi et al., 2014; Greve et al., 2016). To keep the processing pipeline consistent among different PET tracers, partial volume correction was not performed on a regional basis. There may be a potential overestimation of the correlation coefficient, but the significance of the current findings is not likely to be hindered, as indicated in other studies (Aiello et al., 2016; Jiao et al., 2019).

The influence of band filtering and normalization for voxel-based BOLD metrics on the BOLD-physiology association is not negligible. Jiao et al., 2019 demonstrates that ALFF-FDG correlation is dependent on denoising methods such as frequency band of filtering and global signal regression. In an attempt to inform the physiological interpretation of

Author Manuscript Author Manuscript Author Manuscript Author Manuscript

the most widely used rsfMRI metrics, the current study implemented a conventional band (0.01 – 0.08 Hz), consistent with previous quantitative studies that identified fALFF/ReHo/MRGlu correlation (Aiello et al., 2016). Also, several studies normalize the rsfMRI metrics with demeaning or z-standardization (Zuo et al., 2013), especially for ALFF, to eliminate inter-subject variation. To investigate the metabolic origin of BOLD metrics, the correlation of original rsfMRI metrics versus PET metrics is reported, with some of the normalized results in the supplementary materials. Interestingly, significant findings in across-subject comparisons are consistent in both original and normalized rsfMRI metrics, indicating that network-specific across-subject correlations are greater than the whole-brain variation in healthy subjects.

During the resting state acquisition of PET scans, subjects were in an eyes-closed condition with ongoing arterial blood sampling, sample-time recording and blood-sample counting. For rsfMRI, a similar eye-closed condition was chosen, although the alertness of the subjects during the 16 min scan was a concern. For rsfMRI, an eyes-open condition is often used, but can induced regional changes in the BOLD signal (Jao, 2013). Even with eye fixation, there is fluctuation in eye position (with attendant BOLD-signal changes) (Fransson, 2014). Given that equivalently reproducible patterns of fMRI have been described for both the eyes-closed and eyes-open conditions (Liu, 2013), the current study used eyes closed condition to keep consistent with the eyes close condition in the preponderance of PET studies. In the MRI preparation, the subjects were instructed to keep their eyes closed and not to move their body, including extremities and eyes. Before the actual acquisition of rsfMRI protocol, the subjects were notified again and asked to confirm with response. Nonetheless, level of alertness is among potential confounding factors in the current design of the resting state PET-MR study.

The sample size of the current study is small as compared with earlier studies. Some initial resting state studies reporting FDG association of ALFF have 54 subjects (Tomasi et al., 2013), 48 subjects (Liang et al., 2013a) and 26 subjects (Aiello et al., 2015). None of the prior studies, however, had all the traditional hemodynamic-metabolic variables measured in the same subject. Thus, the current dataset is unique, reporting a complete set of PET metabolic (MRGlu MRO_2), hemodynamic (BF, BV) and multi-band resting-state fMRI in each subject. Also, the PET and rs-fMRI measurements were not acquired simultaneously, even though confounding metabolic variables (diet, caffeine, activity condition during scans, time of day, etc) are largely restricted.

The current study implemented mutual information analyses mainly as a descriptive tool supplementary to correlation methods, while second-level mutual information analyses can further inform causality. The contribution of global and different vessel BOLD signals to the resting-state functional connectivity can also be decomposed with conditional mutual information analyses (Colenbier et al., 2020). The causality (i.e directionality) of BV/MRO2 on BF can be inferred with transfer entropy and mutual information analyses (Nourhashemi et al., 2017). With conditional mutual information of BF in the current dataset, blood flow information in BOLD metrics was considered as a result of BOLD-metabolic correspondence, rather than an origin. Indeed, the mutual information approach for directed causality inference is being actively developed (Young et al., 2021; Varley, 2021), and is

Author Manuscript Author Manuscript Author Manuscript Author Manuscript

not yet validated in large-scale multi-modality neuroimaging dataset. Therefore, the current study emphasized mutual information descriptions of the multi-linear relation between BOLD metrics, brain hemodynamics and metabolism.

Finally, extension of the current work should explore the hemodynamic-metabolic correspondence of rsfMRI indices in a dynamic manner, including simultaneous acquisition using PET/MRI. Also, regional and network-specific hemodynamic-metabolic inferences regarding rsfMRI are needed for a more comprehensive and concrete physiological interpretation. In agreement with recent reports from Wang et al. (Wang, 2021), the regional disagreement of MRGlu and fALFF/ReHo, superimposing the overall BOLD-metabolic concordance, calls for further investigation. Current findings of non-flow coupled metabolic information in fALFF and ReHo needs future studies to characterize the exact relationship.

5. Conclusions

Consistent with previous studies, the current study detailed across-region correlations of static ALFF, fractional ALFF and ReHo versus voxel-based hemodynamic and metabolic variables. The current study provided strong evidence that hemodynamic features in the voxel-based BOLD signal at rest are reflective of underlying metabolic demand. Further, non-flow-coupled metabolic information in fALFF and ReHo was identified. The findings in the current study supports the notion that fALFF and ReHo can be considered as metabolic proxies.

Supplementary Material

Refer to Web version on PubMed Central for supplementary material.

Acknowledgements

This work was supported by awards from the United States National Institutes of Health (R01 MH084021, R01 MH-074457 and P30 AG066546). We would like to thank Research Computing Support Group at UTSA for assistance in computation resources. This work received computational support from UTSA's HPC cluster SHAMU, operated by the Office of Information Technology. We thank Dr. Geoffrey D. Clarke for editing suggestions.

Data and code availability statement

The data that support the findings of this study are available from the corresponding author, P.T.F, upon reasonable request. The code used in analyzing mutual information is available at a public repository, https://github.com/robince/gcmi. The toolboxes used in preprocessing (FSL) and analyzing resting state metrics (DPARSF) are available to the community at a public repository, https://fsl.fmrib.ox.ac.uk/fsl/fslwiki/ and http://rfmri.org/DPARSF. The code used to analyze PET data is available from the corresponding author, P.T.F, upon reasonable request.

Abbreviations:

ALFF	amplitude of low frequency fluctuations

Author Manuscript Author Manuscript Author Manuscript Author Manuscript

ReHo	regional homogeneity
fALFF	fractional amplitude of low frequency fluctuations
MRGlu	metabolic rate of glucose
MRO_2	metabolic rate of oxygen
BF	blood flow
BV	blood volume
FDG	fluorodeoxyglucose
MRI	magnetic resonance imaging
PET	positron emission tomography
rsfMRI	resting state functional magnetic resonance imaging
BOLD	blood oxygenation level dependent
EPI	echoplanar imaging
MI	mutual information
II	interaction information
GCMI	gaussian-copula mutual information
GM	gray matter
WM	white matter
F	female
M	male
AAL	automated anatomical labelling (atlas)
MNI	montreal neurological institute (atlas)
ROI	region of interest
Ya	arterial oxygen saturation
VBP	voxel-based physiology

References

Aiello M, Cavaliere C, Salvatore M, 2016. Hybrid PET/MR imaging and brain connectivity. Front. Neurosci. 10, 64. [PubMed: 26973446]

Aiello M, Salvatore E, Cachia A, Pappata S, Cavaliere C, Prinster A, Nicolai E, Salvatore M, Baron JC, Quarantelli M, 2015. Relationship between simultaneously acquired resting-state regional cerebral glucose metabolism and functional MRI: a PET/MR hybrid scanner study. Neuroimage 113, 111–121. [PubMed: 25791784]

Author Manuscript Author Manuscript Author Manuscript Author Manuscript

Alexander-Bloch AF, Shou H, Liu S, Satterthwaite TD, Glahn DC, Shinohara RT, Vandekar SN,Raznahan A, 2018. On testing for spatial correspondence between maps of human brain structure and function. Neuroimage 178, 540–551. [PubMed: 29860082]

Andersen FL, Ladefoged CN, Beyer T, Keller SH, Hansen AE, Hojgaard L, Kjaer A, Law I, Holm S, 2014. Combined PET/MR imaging in neurology: MR-based attenuation correction implies a strong spatial bias when ignoring bone. Neuroimage 84, 206–216. [PubMed: 23994317]

Ashburner J, 2007. A fast diffeomorphic image registration algorithm. Neuroimage 38 (1), 95–113. [PubMed: 17761438]

Beckmann CF, DeLuca M, Devlin JT, Smith SM, 2005. Investigations into resting-state connectivity using independent component analysis. Philos. Trans. R. Soc. B Biol. Sci. 360, 1001–1013.

Behzadi Y, Restom K, Liau J, Liu TT, 2007. A component based noise correction method (CompCor) for BOLD and perfusion based fMRI. Neuroimage 37, 90–101. [PubMed: 17560126]

Bernier M, Croteau E, Castellano CA, Cunnane SC, Whittingstall K, 2017. Spatial distribution of resting-state BOLD regional homogeneity as a predictor of brain glucose uptake: a study in healthy aging. Neuroimage 150, 14–22. [PubMed: 28130193]

Bettinardi V, Castiglioni I, De Bernardi E, Gilardi M, 2014. PET quantification: strategies for partial volume correction. Clin. Transl. Imaging 2, 199–218.

Bing X, Ming-Guo Q, Ye Z, Jing-Na Z, Min L, Han C, Yu Z, Jia-Jia Z, Jian W, Wei C, Han-Jian D, Shao-Xiang Z, 2013. Alterations in the cortical thickness and the amplitude of low-frequency fluctuation in patients with post-traumatic stress disorder. Brain Res. 1490, 225–232. [PubMed: 23122880]

Birn RM, Diamond JB, Smith MA, Bandettini PA, 2006. Separating respiratory-variation-related fluctuations from neuronal-activity-related fluctuations in fMRI. Neuroimage 31, 1536–1548. [PubMed: 16632379]

Birn RM, Molloy EK, Patriat R, Parker T, Meier TB, Kirk GR, Nair VA, Meyerand ME, Prabhakaran V, 2013. The effect of scan length on the reliability of resting-state fMRI connectivity estimates. Neuroimage 83, 550–558. [PubMed: 23747458]

Birn RM, Smith MA, Jones TB, Bandettini PA, 2008. The respiration response function: the temporal dynamics of fMRI signal fluctuations related to changes in respiration. Neuroimage 40, 644–654. [PubMed: 18234517]

Biswal B, Yetkin FZ, Haughton VM, Hyde JS, 1995. Functional connectivity in the motor cortex of resting human brain using echo-planar MRI. Magn. Reson. Med. 34, 537–541. [PubMed: 8524021]

Brickman AM, Small SA, Fleisher A, 2009. Pinpointing synaptic loss caused by Alzheimer's disease with fMRI. Behav. Neurol. 21, 93–100. [PubMed: 19847048]

Bright MG, Whittaker JR, Driver ID, Murphy K, 2020. Vascular physiology drives functional brain networks. Neuroimage 217, 116907. [PubMed: 32387624]

Bumstead JR, Bauer AQ, Wright PW, Culver JP, 2017. Cerebral functional connectivity and Mayer waves in mice: phenomena and separability. J. Cereb. Blood Flow Metab. 37, 471–484. [PubMed: 26868180]

Buxton RB, Wong EC, Frank LR, 1998. Dynamics of blood flow and oxygenation changes during brain activation: the balloon model. Magn. Reson. Med. 39, 855–864. [PubMed: 9621908]

Carré A, Klausner G, Edjlali M, Lerousseau M, Briend-Diop J, Sun R, Ammari S, Reuzé S, Andres EA, Estienne T, 2020. Standardization of brain MR images across machines and protocols: bridging the gap for MRI-based radiomics. Sci. Rep. 10, 1–15. [PubMed: 31913322]

Chang C, Cunningham JP, Glover GH, 2009. Influence of heart rate on the BOLD signal: the cardiac response function. Neuroimage 44, 857–869. [PubMed: 18951982]

Chang C, Glover GH, 2009a. Effects of model-based physiological noise correction on default mode network anti-correlations and correlations. Neuroimage 47, 1448–1459. [PubMed: 19446646]

Chang C, Glover GH, 2009b. Relationship between respiration, end-tidal CO2, and BOLD signals in resting-state fMRI. Neuroimage 47, 1381–1393. [PubMed: 19393322]

Chen JE, Lewis LD, Chang C, Tian Q, Fultz NE, Ohringer NA, Rosen BR, Polimeni JR, 2020. Resting-state "physiological networks. Neuroimage 213, 116707. [PubMed: 32145437]

Author Manuscript Author Manuscript Author Manuscript Author Manuscript

Cho J, Lee J, An H, Goyal MS, Su Y, Wang Y, 2020. Cerebral oxygen extraction fraction (OEF): Comparison of challenge-free gradient echo QSM+ qBOLD (QQ) with 15O PET in healthy adults. J. Cereb. Blood Flow Metab. 41 (7), 1658–1668 0271678X20973951. [PubMed: 33243071]

Cole DM, Smith SM, Beckmann CF, 2010. Advances and pitfalls in the analysis and interpretation of resting-state FMRI data. Front. Syst. Neurosci. 4, 8. [PubMed: 20407579]

Colenbier N, Van de Steen F, Uddin LQ, Poldrack RA, Calhoun VD, Marinazzo D, 2020. Disambiguating the role of blood flow and global signal with partial information decomposition. Neuroimage 213, 116699. [PubMed: 32179104]

Cordes D, Haughton VM, Arfanakis K, Wendt GJ, Turski PA, Moritz CH, Quigley MA, Meyerand ME, 2000. Mapping functionally related regions of brain with functional connectivity MR imaging. AJNR Am. J. Neuroradiol. 21, 1636–1644. [PubMed: 11039342]

Cortese S, Aoki YY, Itahashi T, Castellanos FX, Eickhoff SB, 2021. Systematic review and meta-analysis: resting-state functional magnetic resonance imaging studies of attention-deficit/hyperactivity disorder. J. Am. Acad. Child Adolesc. Psychiatry 60, 61–75. [PubMed: 32946973]

Di X, Biswal BB, 2017. Psychophysiological interactions in a visual checkerboard task: reproducibility, reliability, and the effects of deconvolution. Front. Neurosci. 11, 573. [PubMed: 29089865]

Davis TL, Kwong KK, Weisskoff RM, Rosen BR, 1998. Calibrated functional MRI: mapping the dynamics of oxidative metabolism. Proceedings of the National Academy of Sciences 95 (4), 1834–1839.

Di X, Biswal BB Alzheimer's Disease Neuroimaging I, 2012. Metabolic brain covariant networks as revealed by FDG-PET with reference to resting-state fMRI networks. Brain Connect 2, 275–283. [PubMed: 23025619]

Di X, Wolfer M, Amend M, Wehrl H, Ionescu TM, Pichler BJ, Biswal BB Alzheimer's Disease Neuroimaging I, 2019. Interregional causal influences of brain metabolic activity reveal the spread of aging effects during normal aging. Hum. Brain Mapp. 40, 4657–4668. [PubMed: 31389641]

Dormann CF, Elith J, Bacher S, Buchmann C, Carl G, Carré G, Marquéz JRG, Gruber B, Lafourcade B, Leitao PJ, 2013. Collinearity: a review of methods to deal with it and a simulation study evaluating their performance. Ecography 36, 27–46.

Ekstrom A, 2010. How and when the fMRI BOLD signal relates to underlying neural activity: the danger in dissociation. Brain Res. Rev. 62, 233–244. [PubMed: 20026191]

Ekstrom AD, 2021. Regional variation in neurovascular coupling and why we still lack a Rosetta Stone. Philos. Trans. R. Soc. B 376, 20190634.

Emblem KE, Nedregaard B, Nome T, Due-Tonnessen P, Hald JK, Scheie D, Borota OC, Cvancarova M, Bjornerud A, 2008. Glioma grading by using histogram analysis of blood volume heterogeneity from MR-derived cerebral blood volume maps. Radiology 247, 808–817. [PubMed: 18487536]

Fan AP, An H, Moradi F, Rosenberg J, Ishii Y, Nariai T, Okazawa H, Zaharchuk G, 2020. Quantification of brain oxygen extraction and metabolism with [15O]-gas PET: A technical review in the era of PET/MRI. Neuroimage 117–136. doi:10.1016/j.neuroimage.2020.117136.

Fan Z, Chen X, Qi ZX, Li L, Lu B, Jiang CL, Zhu RQ, Yan CG, Chen L, 2019. Physiological significance of R-fMRI indices: Can functional metrics differentiate structural lesions (brain tumors)? NeuroImage Clin. 22, 101741. [PubMed: 30878611]

Fonov VS, Evans AC, McKinstry RC, Almli C, Collins D, 2009. Unbiased nonlinear average age-appropriate brain templates from birth to adulthood. Neuroimage S102.

Fox PT, Lancaster JL, Laird AR, Eickhoff SB, 2014. Meta-analysis in human neuroimaging: computational modeling of large-scale databases. Annu. Rev. Neurosci. 37, 409–434. [PubMed: 25032500]

Fox PT, Raichle ME, 1986. Focal physiological uncoupling of cerebral blood flow and oxidative metabolism during somatosensory stimulation in human subjects. Proc. Natl. Acad. Sci. 83, 1140–1144. [PubMed: 3485282]

Fransson P, Flodin P, Seimyr GÖ, Pansell T, 2014. Slow fluctuations in eye position and resting-state functional magnetic resonance imaging brain activity during visual fixation. European Journal of Neuroscience 40 (12), 3828–3835. [PubMed: 25302817]

Author Manuscript Author Manuscript Author Manuscript Author Manuscript

Frederick B.d., Nickerson LD, Tong Y, 2012. Physiological denoising of BOLD fMRI data using Regressor Interpolation at Progressive Time Delays (RIPTiDe) processing of concurrent fMRI and near-infrared spectroscopy (NIRS). Neuroimage 60, 1913–1823. [PubMed: 22342801]

Friston KJ, Williams S, Howard R, Frackowiak RS, Turner R, 1996. Movement-related effects in fMRI time-series. Magnetic resonance in medicine 35 (3), 346–355. [PubMed: 8699946]

Fu C, Zhang H, Xuan A, Gao Y, Xu J, Shi D, 2018. A combined study of (18)F-FDG PET-CT and fMRI for assessing resting cerebral function in patients with major depressive disorder. Exp. Ther. Med. 16, 1873–1881. [PubMed: 30186413]

Fukunaga M, Horovitz SG, de Zwart JA, van Gelderen P, Balkin TJ, Braun AR, Duyn JH, 2008. Metabolic origin of BOLD signal fluctuations in the absence of stimuli. J. Cereb. Blood Flow Metab. 28, 1377–1387. [PubMed: 18382468]

Garrett DD, Samanez-Larkin GR, MacDonald SW, Lindenberger U, McIntosh AR, Grady CL, 2013a. Moment-to-moment brain signal variability: a next frontier in human brain mapping? Neurosci. Biobehav. Rev. 37, 610–624. [PubMed: 23458776]

Gauthier CJ, Madjar C, Desjardins-Crepeau L, Bellec P, Bherer L, Hoge RD, 2013. Age dependence of hemodynamic response characteristics in human functional magnetic resonance imaging. Neurobiol. Aging 34, 1469–1485. [PubMed: 23218565]

Ghassami AmirEmad, Kiyavash Negar, 2017. Interaction information for causal inference: The case of directed triangle. 2017 IEEE International Symposium on Information Theory (ISIT) 1326–1330.

Girouard H, Iadecola C, 2006. Neurovascular coupling in the normal brain and in hypertension, stroke, and Alzheimer disease. J. Appl. Physiol. 100, 328–335 (1985). [PubMed: 16357086]

Golanov EV, Yamamoto S, Reis DJ, 1994. Spontaneous waves of cerebral blood flow associated with a pattern of electrocortical activity. Am. J. Physiol. 266, R204–R214. [PubMed: 8304543]

Grandin CB, Bol A, Smith AM, Michel C, Cosnard G, 2005. Absolute CBF and CBV measurements by MRI bolus tracking before and after acetazolamide challenge: repeatabilily and comparison with PET in humans. Neuroimage 26, 525–535. [PubMed: 15907309]

Gray JP, Muller VI, Eickhoff SB, Fox PT, 2020. Multimodal abnormalities of brain structure and function in major depressive disorder: a meta-analysis of neuroimaging studies. Am. J. Psychiatry 177, 422–434. [PubMed: 32098488]

Greve DN, Salat DH, Bowen SL, Izquierdo-Garcia D, Schultz AP, Catana C, Becker JA, Svarer C, Knudsen GM, Sperling RA, Johnson KA, 2016. Different partial volume correction methods lead to different conclusions: An (18)F-FDG-PET study of aging. Neuroimage 132, 334–343. [PubMed: 26915497]

Grubb RL, Raichle ME, Higgins CS, Eichling JO, 1978. Measurement of regional cerebral blood volume by emission tomography. Ann. Neurol. Off. J. Am. Neurol. Assoc. Child Neurol. Soc. 4, 322–328.

Grubb RL, Phelps ME, Ter-Pogossian MM, 1973. Regional cerebral blood volume in humans: x-ray fluorescence studies. Arch. Neurol. 28, 38–44. [PubMed: 4629381]

Han Y, Wang J, Zhao Z, Min B, Lu J, Li K, He Y, Jia J, 2011. Frequency-dependent changes in the amplitude of low-frequency fluctuations in amnestic mild cognitive impairment: a resting-state fMRI study. Neuroimage 55, 287–295. [PubMed: 21118724]

Haroon E, Chen X, Li Z, Patel T, Woolwine BJ, Hu XP, Felger JC, Miller AH, 2018. Increased inflammation and brain glutamate define a subtype of depression with decreased regional homogeneity, impaired network integrity, and anhedonia. Transl. Psychiatry 8, 1–11. [PubMed: 29317594]

Heeger DJ, Ress D, 2002. What does fMRI tell us about neuronal activity? Nat. Rev. Neurosci. 3, 142–151. [PubMed: 11836522]

Henriksen OM, Gjedde A, Vang K, Law I, Aanerud J, Rostrup E, 2021. Regional and interindividual relationships between cerebral perfusion and oxygen metabolism. J. Appl. Physiol. 130 (6), 1836–1847. doi:10.1152/japplphysiol.00939.2020. [PubMed: 33830816]

Hillman EM, 2014. Coupling mechanism and significance of the BOLD signal: a status report. Annu. Rev. Neurosci. 37, 161–181. [PubMed: 25032494]

Hitz S, Habekost C, Furst S, Delso G, Forster S, Ziegler S, Nekolla SG, Souvat-zoglou M, Beer AJ, Grimmer T, Eiber M, Schwaiger M, Drzezga A, 2014. Systematic comparison of the performance

Author Manuscript Author Manuscript Author Manuscript Author Manuscript

of integrated whole-body PET/MR imaging to conventional PET/CT for (1)(8)F-FDG brain imaging in patients examined for suspected dementia. J. Nucl. Med. 55, 923–931. [PubMed: 24833495]

Hou Y, Wu X, Hallett M, Chan P, Wu T, 2014. Frequency-dependent neural activity in Parkinson's disease. Hum. Brain Mapp. 35, 5815–5833. [PubMed: 25045127]

Huettel SA, Song AW, McCarthy G, 2004. Functional magnetic resonance imaging. Sinauer Associates Sunderland, MA.

Huisman MC, van Golen LW, Hoetjes NJ, Greuter HN, Schober P, Ijzerman RG, Diamant M, Lammertsma AA, 2012. Cerebral blood flow and glucose metabolism in healthy volunteers measured using a high-resolution PET scanner. EJNMMI research 2 (1), 1–9. [PubMed: 22251281]

Hyder F, Herman P, Bailey CJ, Møller A, Globinsky R, Fulbright RK, Rothman DL, Gjedde A, 2016. Uniform distributions of glucose oxidation and oxygen extraction in gray matter of normal human brain: no evidence of regional differences of aerobic glycolysis. Journal of Cerebral Blood Flow & Metabolism 36 (5), 903–916. [PubMed: 26755443]

Iida H, Kanno I, Takahashi A, Miura S, Murakami M, Takahashi K, Ono Y, Shishido F, Inugami A, Tomura N, 1988. Measurement of absolute myocardial blood flow with H215O and dynamic positron-emission tomography. Strategy for quantification in relation to the partial-volume effect. Circulation 78 (1), 104–115. doi:10.1161/01.CIR.78.1.104. [PubMed: 3260151]

Iida H, Kanno I, Miura S, 1991. Rapid measurement of cerebral blood flow with positron emission tomography. Ciba Found. Symp. 163, 23–37 discussion 37–42. [PubMed: 1815893]

Ince RA, Giordano BL, Kayser C, Rousselet GA, Gross J, Schyns PG, 2017a. A statistical framework for neuroimaging data analysis based on mutual information estimated via a gaussian copula. Hum. Brain Mapp. 38, 1541–1573. [PubMed: 27860095]

Ishii Y, Thamm T, Guo J, Khalighi MM, Wardak M, Holley D, Gandhi H, Park JH, Shen B, Steinberg GK, 2020. Simultaneous phase-contrast MRI and PET for noninvasive quantification of cerebral blood flow and reactivity in healthy subjects and patients with cerebrovascular disease. Journal of Magnetic Resonance Imaging 51 (1), 183–194 [PubMed: 31044459]

Jao T, Vértes PE, Alexander-Bloch AF, Tang I-N, Yu Y-C, Chen J-H, Bullmore ET, 2013. Volitional eyes opening perturbs brain dynamics and functional connectivity regardless of light input. Neuroimage 69, 21–34. [PubMed: 23266698]

Jenkinson M, Bannister P, Brady M, Smith S, 2002. Improved optimization for the robust and accurate linear registration and motion correction of brain images. Neuroimage 17, 825–841. [PubMed: 12377157]

Jenkinson M, Smith S, 2001. A global optimisation method for robust affine registration of brain images. Med. Image Anal. 5, 143–156. [PubMed: 11516708]

Jiang D, Deng S, Franklin CG, O'Boyle M, Zhang W, Heyl BL, Pan L, Jerabek PA, Fox PT, Lu H, 2021. Validation of T2-based oxygen extraction fraction measurement with 15O positron emission tomography. Magn. Reson. Med. 85, 290–297. [PubMed: 32643207]

Jiang L, Zuo XN, 2016. Regional homogeneity: a multimodal, multiscale neuroimaging marker of the human connectome. Neuroscientist 22, 486–505. [PubMed: 26170004]

Jiao F, Gao Z, Shi K, Jia X, Wu P, Jiang C, Ge J, Su H, Guan Y, Shi S, 2019. Frequency-dependent relationship between resting-state fMRI and glucose metabolism in the elderly. Front. Neurol. 10, 566. [PubMed: 31191447]

Kasper L, Bollmann S, Diaconescu AO, Hutton C, Heinzle J, Iglesias S, Hauser TU, Sebold M, Manjaly ZM, Pruessmann KP, 2017. The PhysIO toolbox for modeling physiological noise in fMRI data. J. Neurosci. Methods 276, 56–72. [PubMed: 27832957]

Kassinopoulos M, Mitsis GD, 2019. Identification of physiological response functions to correct for fluctuations in resting-state fMRI related to heart rate and respiration. Neuroimage 202, 116150. [PubMed: 31487547]

Kim SG, Hendrich K, Hu X, Merkle H, Ugurbil K, 1994. Potential pitfalls of functional MRI using conventional gradient-recalled echo techniques. NMR Biomed. 7, 69–74. [PubMed: 8068528]

Kudo K, Terae S, Katoh C, Oka M, Shiga T, Tamaki N, Miyasaka K, 2003. Quantitative cerebral blood flow measurement with dynamic perfusion CT using the vascular-pixel elimination method:

Author Manuscript Author Manuscript Author Manuscript Author Manuscript

comparison with H2(15)O positron emission tomography. AJNR Am. J. Neuroradiol. 24, 419–426. [PubMed: 12637292]

Kundu P, Inati SJ, Evans JW, Luh W-M, Bandettini PA, 2012. Differentiating BOLD and non-BOLD signals in fMRI time series using multi-echo EPI. Neuroimage 60, 1759–1770. [PubMed: 22209809]

Lau WKW, Leung MK, Lau BWM, 2019. Resting-state abnormalities in autism spectrum disorders: a meta-analysis. Sci. Rep. 9, 3892. [PubMed: 30846796]

Lenz C, Frietsch T, Fütterer C, Rebel A, van Ackern K, Kuschinsky W, Waschke KF, 1999. Local coupling of cerebral blood flow to cerebral glucose metabolism during inhalational anesthesia in rats desflurane versus isoflurane. Anesthesiol. J. Am. Soc. Anesthesiol. 91, 1720–1720.

Lenz C, Rebel A, van Ackern K, Kuschinsky W, Waschke KF, 1998. Local cerebral blood flow, local cerebral glucose utilization, and flow-metabolism coupling during sevoflurane versus isoflurane anesthesia in rats. Anesthesiol. J. Am. Soc. Anesthesiol. 89, 1480–1488.

Lewis N, Lu H, Liu P, Hou X, Damaraju E, Iraji A, Calhoun V, 2020. Static and dynamic functional connectivity analysis of cerebrovascular reactivity: An fMRI study. Brain Behav. 10, e01516. [PubMed: 32342644]

Li C, Liu C, Yin X, Yang J, Gui L, Wei L, Wang J, 2014. Frequency-dependent changes in the amplitude of low-frequency fluctuations in subcortical ischemic vascular disease (SIVD): a resting-state fMRI study. Behav. Brain Res. 274, 205–210. [PubMed: 25138697]

Li SJ, Li Z, Wu G, Zhang MJ, Franczak M, Antuono PG, 2002. Alzheimer disease: evaluation of a functional MR imaging index as a marker. Radiology 225, 253–259. [PubMed: 12355013]

Li Z, Kadivar A, Pluta J, Dunlop J, Wang Z, 2012a. Test-retest stability analysis of resting brain activity revealed by blood oxygen level-dependent functional MRI. J. Magn. Reson. Imaging 36, 344–354. [PubMed: 22535702]

Li Z, Zhu Y, Childress AR, Detre JA, Wang Z, 2012b. Relations between BOLD fMRI-derived resting brain activity and cerebral blood flow. PLoS One 7, e44556. [PubMed: 23028560]

Liang X, Zou Q, He Y, Yang Y, 2013a. Coupling of functional connectivity and regional cerebral blood flow reveals a physiological basis for network hubs of the human brain. Proc. Natl. Acad. Sci. USA 110, 1929–1934. [PubMed: 23319644]

Liu D, Dong Z, Zuo X, Wang J, Zang Y, 2013. Eyes-open/eyes-closed dataset sharing for reproducibility evaluation of resting state fMRI data analysis methods. Neuroin-formatics 11 (4), 469–476.

Liu P, Li Y, Pinho M, Park DC, Welch BG, Lu H, 2017. Cerebrovascular reactivity mapping without gas challenges. Neuroimage 146, 320–326. [PubMed: 27888058]

Lv H, Wang Z, Tong E, Williams LM, Zaharchuk G, Zeineh M, Goldstein-Piekarski AN, Ball TM, Liao C, Wintermark M, 2018. Resting-state functional MRI: everything that nonexperts have always wanted to know. Am. J. Neuro-radiol. 39, 1390–1399.

Maes F, Collignon A, Vandermeulen D, Marchal G, Suetens P, 1997. Multimodality image registration by maximization of mutual information. IEEE Trans. Med. Imaging 16, 187–198. [PubMed: 9101328]

Magistretti PJ, Pellerin L, Rothman DL, Shulman RG, 1999. Energy on demand. Science 283, 496–497. [PubMed: 9988650]

Magri C, Schridde U, Murayama Y, Panzeri S, Logothetis NK, 2012. The amplitude and timing of the BOLD signal reflects the relationship between local field potential power at different frequencies. J. Neurosci. 32, 1395–1407. [PubMed: 22279224]

Markello RD, Misic B, 2021. Comparing spatial null models for brain maps. NeuroImage 236, 118052. [PubMed: 33857618]

Martin WR, Powers WJ, Raichle ME, 1987. Cerebral blood volume measured with inhaled C15O and positron emission tomography. J. Cereb. Blood Flow Metab. 7, 421–426. [PubMed: 3497162]

Mayhew JE, Askew S, Zheng Y, Porrill J, Westby GW, Redgrave P, Rector DM, Harper RM, 1996. Cerebral vasomotion: a 0.1-Hz oscillation in reflected light imaging of neural activity. Neuroimage 4, 183–193. [PubMed: 9345508]

Mintun M, Raichle M, Martin W, Herscovitch P, 1984. Brain oxygen utilization measured with 0–15 radiotracers and positron emission tomography. J. Nucl. Med. 25, 177–187. [PubMed: 6610032]

Author Manuscript Author Manuscript Author Manuscript Author Manuscript

Mueller S, Wang D, Fox MD, Yeo BT, Sepulcre J, Sabuncu MR, Shafee R, Lu J, Liu H, 2013. Individual variability in functional connectivity architecture of the human brain. Neuron 77, 586–595. [PubMed: 23395382]

Murphy K, Fox MD, 2017. Towards a consensus regarding global signal regression for resting state functional connectivity MRI. Neuroimage 154, 169–173. [PubMed: 27888059]

Narciso L, Ssali T, Anazodo U, Iida H, St Lawrence K, 2021. A non-invasive reference-based method for imaging the cerebral metabolic rate of oxygen by PET/MR: theory and error analysis. Physics in Medicine & Biology 66 (6), 065009. [PubMed: 33596555]

Nourhashemi M, Mahmoudzadeh M, Goudjil S, Kongolo G, Wallois F, 2020. Neurovascular coupling in the developing neonatal brain at rest. Human brain mapping 41 (2), 503–519. doi:10.1002/hbm.24818. [PubMed: 31600024]

Nugent AC, Martinez A, D'alfonso A, Zarate CA, Theodore WH, 2015. The relationship between glucose metabolism, resting-state fMRI BOLD signal, and GABAA-binding potential: a preliminary study in healthy subjects and those with temporal lobe epilepsy. J. Cereb. Blood Flow Metab. 35, 583–591. [PubMed: 25564232]

Nourhashemi M, Kongolo G, Mahmoudzadeh M, Goudjil S, Wallois F, 2017. Relationship between relative cerebral blood flow, relative cerebral blood volume, and relative cerebral metabolic rate of oxygen in the preterm neonatal brain. Neurophotonics 4, 021104. [PubMed: 28439520]

Nugent S, Croteau E, Potvin O, Castellano C-A, Dieumegarde L, Cunnane SC, Duchesne S, 2020. Selection of the optimal intensity normalization region for FDG-PET studies of normal aging and Alzheimer's disease. Sci. Rep. 10, 1–8. [PubMed: 31913322]

Olbrich E, Bertschinger N, Rauh J, 2015. Information decomposition and synergy. Entropy 17 (5), 3501–3507.

Pathak AP, Schmainda KM, Ward BD, Linderman JR, Rebro KJ, Greene AS, 2001. MR-derived cerebral blood volume maps: issues regarding histological validation and assessment of tumor angiogenesis. Magn. Reson. Med. 46, 735–747. [PubMed: 11590650]

Phelps ME, Huang S, Hoffman E, Selin C, Sokoloff L, Kuhl DE, 1979. Tomographic measurement of local cerebral glucose metabolic rate in humans with (F-18) 2-fluoro-2-deoxy-D-glucose: validation of method. Ann. Neurol. Off. J. Am. Neurol. Assoc. Child Neurol. Soc. 6, 371–388.

Phillips AA, Chan FH, Zheng MMZ, Krassioukov AV, Ainslie PN, 2016. Neurovascular coupling in humans: physiology, methodological advances and clinical implications. J. Cereb. Blood Flow. Metab. 36, 647–664. [PubMed: 26661243]

Power JD, Plitt M, Gotts SJ, Kundu P, Voon V, Bandettini PA, Martin A, 2018. Ridding fMRI data of motion-related influences: removal of signals with distinct spatial and physical bases in multiecho data. Proc. Natl. Acad. Sci. 115, E2105–E2114. [PubMed: 29440410]

Power JD, Plitt M, Laumann TO, Martin A, 2017. Sources and implications of whole-brain fMRI signals in humans. Neuroimage 146, 609–625. [PubMed: 27751941]

Prokopiou PC, Pattinson KT, Wise RG, Mitsis GD, 2019. Modeling of dynamic cerebrovascular reactivity to spontaneous and externally induced CO_2 fluctuations in the human brain using BOLD-fMRI. Neuroimage 186, 533–548. [PubMed: 30423427]

Pruim RH, Mennes M, van Rooij D, Llera A, Buitelaar JK, Beckmann CF, 2015. ICA-AROMA: A robust ICA-based strategy for removing motion artifacts from fMRI data. Neuroimage 112, 267–277. [PubMed: 25770991]

Qing Z, Dong Z, Li S, Zang Y, Liu D, 2015. Global signal regression has complex effects on regional homogeneity of resting state fMRI signal. Magn. Reson. Imaging 33, 1306–1313. [PubMed: 26234499]

Raichle ME, 1998. Behind the scenes of functional brain imaging: a historical and physiological perspective. Proc. Natl. Acad. Sci. USA 95, 765–772. [PubMed: 9448239]

Raichle ME, Martin W, Herscovitch P, Mintun M, Markham J, 1983. Brain blood flow measured with intravenous H2 (15) O. II. Implementation and validation. J. Nucl. Med. 24, 790–798. [PubMed: 6604140]

Raichle ME, Mintun MA, 2006. Brain work and brain imaging. Annu. Rev. Neurosci. 29, 449–476. [PubMed: 16776593]

Author Manuscript Author Manuscript Author Manuscript Author Manuscript

Razavi M, Eaton B, Paradiso S, Mina M, Hudetz AG, Bolinger L, 2008. Source of low-frequency fluctuations in functional MRI signal. J. Magn. Reson. Imaging 27, 891–897. [PubMed: 18383250]

Rocher AB, Chapon F, Blaizot X, Baron J-C, Chavoix C, 2003. Resting-state brain glucose utilization as measured by PET is directly related to regional synaptophysin levels: a study in baboons. Neuroimage 20, 1894–1898. [PubMed: 14642499]

Rosas FE, Mediano PAM, Gastpar M, Jensen HJ, 2019. Quantifying high-order interdependencies via multivariate extensions of the mutual information. Phys. Rev. E 100, 032305. [PubMed: 31640038]

Roy CS, Sherrington CS, 1890. On the regulation of the blood-supply of the brain. J. Physiol. 11, 85.

Salvador R, Martinez A, Pomarol-Clotet E, Sarro S, Suckling J, Bullmore E, 2007. Frequency based mutual information measures between clusters of brain regions in functional magnetic resonance imaging. Neuroimage 35, 83–88. [PubMed: 17240167]

Schmidt K, Lucignani G, Moresco R, Rizzo G, Gilardi M, Messa C, Colombo F, Fazio F, Sokoloff L, 1992. Errors introduced by tissue heterogeneity in estimation of local cerebral glucose utilization with current kinetic models of the [18F] fluorodeoxyglucose method. J. Cereb. Blood Flow Metab. 12, 823–834. [PubMed: 1506447]

Schyns PG, Thut G, Gross J, 2011. Cracking the code of oscillatory activity. PLoS Biol. 9, el001064.

Sha Z, Xia M, Lin Q, Cao M, Tang Y, Xu K, Song H, Wang Z, Wang F, Fox PT, 2018. Meta-connectomic analysis reveals commonly disrupted functional architectures in network modules and connectors across brain disorders. Cereb. Cortex 28, 4179–4194. [PubMed: 29136110]

Shannon BJ, Vaishnavi SN, Vlassenko AG, Shimony JS, Rutlin J, Raichle ME, 2016. Brain aerobic glycolysis and motor adaptation learning. Proc. Natl. Acad. Sci. 113, E3782–E3791. [PubMed: 27217563]

Shaw K, Bell L, Boyd K, Grijseels D, Clarke D, Bonnar O, Crombag H, Hall C, 2021. Neurovascular coupling and oxygenation are decreased in hippocampus compared to neocortex because of microvascular differences. Nat. Commun. 12, 1–16. [PubMed: 33397941]

Shen J, 2013. Modeling the glutamate–glutamine neurotransmitter cycle. Front. Neuroenerg. 5, 1.

Shen J, Petersen KF, Behar KL, Brown P, Nixon TW, Mason GF, Petroff OA, Shulman GI, Shulman RG, Rothman DL, 1999. Determination of the rate of the glutamate/glutamine cycle in the human brain by in vivo 13C NMR. Proc. Natl. Acad. Sci. 96, 8235–8240. [PubMed: 10393978]

Shmueli K, van Gelderen P, de Zwart JA, Horovitz SG, Fukunaga M, Jansma JM, Duyn JH, 2007. Low-frequency fluctuations in the cardiac rate as a source of variance in the resting-state fMRI BOLD signal. Neuroimage 38, 306–320. [PubMed: 17869543]

Shokri-Kojori E, Tomasi D, Alipanahi B, Wiers CE, Wang G-J, Volkow ND, 2019. Correspondence between cerebral glucose metabolism and BOLD reveals relative power and cost in human brain. Nat. Commun. 10, 1–12. [PubMed: 30602773]

Small SA, 2003. Measuring correlates of brain metabolism with high-resolution MRI: a promising approach for diagnosing Alzheimer disease and mapping its course. Alzheimer Dis. Assoc. Disord. 17, 154–161. [PubMed: 14512829]

Song L, Langfelder P, Horvath S, 2012. Comparison of co-expression measures: mutual information, correlation, and model based indices. BMC Bioinform. 13, 328.

Stoessl AJ, 2017. Glucose utilization: still in the synapse. Nat. Neurosci. 20, 382–384. [PubMed: 28230843]

Taylor PA, Gohel S, Di X, Walter M, Biswal BB, 2012. Functional covariance networks: obtaining resting-state networks from intersubject variability. Brain Connect 2, 203–217. [PubMed: 22765879]

Tomasi D, Volkow ND, 2010a. Functional connectivity density mapping. Proc. Natl. Acad. Sci. 107, 9885–9890. [PubMed: 20457896]

Tomasi D, Wang GJ, Volkow ND, 2013. Energetic cost of brain functional connectivity. Proc. Natl. Acad. Sci. USA 110, 13642–13647. [PubMed: 23898179]

Tremblay S, Beaulé V, Proulx S, De Beaumont L, Marjańska M, Doyon J, Pascual-Leone A, Lassonde M, Théoret H, 2013. Relationship between transcranial magnetic stimulation measures

Author Manuscript Author Manuscript Author Manuscript Author Manuscript

of intracortical inhibition and spectroscopy measures of GABA and glutamate+ glutamine. J. Neurophysiol. 109, 1343–1349. [PubMed: 23221412]

Turner R, 2002. How much cortex can a vein drain? Downstream dilution of activation-related cerebral blood oxygenation changes. Neuroimage 16, 1062–1067. [PubMed: 12202093]

Vaishnavi SN, Vlassenko AG, Rundle MM, Snyder AZ, Mintun MA, Raichle ME, 2010. Regional aerobic glycolysis in the human brain. Proc. Natl. Acad. Sci. 107, 17757–17762. [PubMed: 20837536]

van Aalst J, Ceccarini J, Sunaert S, Dupont P, Koole M, Van Laere K, 2021. In vivo synaptic density relates to glucose metabolism at rest in healthy subjects, but is strongly modulated by regional differences. J. Cereb. Blood Flow Metab. 41 (8), 1978–1987 0271678X20981502. [PubMed: 33444094]

Varley TF, 2021. Intersectional synergies: untangling irreducible effects of intersecting identities via information decomposition. arXiv preprint arXiv:2106.10338.

Verstynen TD, Deshpande V, 2011. Using pulse oximetry to account for high and low frequency physiological artifacts in the BOLD signal. Neuroimage 55, 1633–1644. [PubMed: 21224001]

Vigneau-Roy N, Bernier M, Descoteaux M, Whittingstall K, 2014. Regional variations in vascular density correlate with resting-state and task-evoked blood oxygen level-dependent signal amplitude. Hum. Brain Mapp. 35, 1906–1920. [PubMed: 23843266]

Wang J, Sun H, Cui B, Yang H, Shan Y, Dong C, Zang Y, Lu J, 2021. The relationship among glucose metabolism, cerebral blood flow, and functional activity: a hybrid pet/fmri study. Molecular Neurobiology 58 (6), 2862–2873. [PubMed: 33523358]

Wehrl HF, Hossain M, Lankes K, Liu CC, Bezrukov I, Martirosian P, Schick F, Reischl G, Pichler BJ, 2013. Simultaneous PET-MRI reveals brain function in activated and resting state on metabolic, hemodynamic and multiple temporal scales. Nat. Med. 19, 1184–1189. [PubMed: 23975025]

Wesolowski R, Blockley NP, Driver ID, Francis ST, Gowland PA, 2019. Coupling between cerebral blood flow and cerebral blood volume: Contributions of different vascular compartments. NMR in Biomedicine 32 (3), e4061. [PubMed: 30657208]

Wesolowski R, Blockley NP, Driver ID, Francis ST, Gowland PA, 2019. Coupling between cerebral blood flow and cerebral blood volume: Contributions of different vascular compartments. NMR Biomed. 32, e4061. [PubMed: 30657208]

Wink AM, Bernard F, Salvador R, Bullmore E, Suckling J, 2006. Age and cholinergic effects on hemodynamics and functional coherence of human hippocampus. Neurobiol. Aging 27, 1395–1404. [PubMed: 16202481]

Winkler AM, Ridgway GR, Webster MA, Smith SM, Nichols TE, 2014. Permutation inference for the general linear model. Neuroimage 92, 381–397. [PubMed: 24530839]

Xia M, Wang J, He Y, 2013. BrainNet viewer: a network visualization tool for human brain connectomics. PLoS One 8, e68910. [PubMed: 23861951]

Xifra-Porxas A, Kassinopoulos M, Mitsis GD, 2021. Physiological and motion signatures in static and time-varying functional connectivity and their subject identifiability. eLife 10, e62324. [PubMed: 34342582]

Xu J, Moeller S, Auerbach EJ, Strupp J, Smith SM, Feinberg DA, Yacoub E, U ğurbil K, 2013. Evaluation of slice accelerations using multiband echo planar imaging at 3 T. Neuroimage 83, 991–1001. [PubMed: 23899722]

Xu Y, Cao M, Liao X, Xia M, Wang X, Jeon T, Ouyang M, Chalak L, Rollins N, Huang H, He Y, 2019. Development and Emergence of Individual Variability in the Functional Connectivity Architecture of the Preterm Human Brain. Cereb. Cortex 29, 4208–4222. [PubMed: 30534949]

Yan CG, Craddock RC, Zuo XN, Zang YF, Milham MP, 2013. Standardizing the intrinsic brain: towards robust measurement of inter-individual variation in 1000 functional connectomes. Neuroimage 80, 246–262. [PubMed: 23631983]

Yan C, Zang Y, 2010. DPARSF: a MATLAB toolbox for" pipeline" data analysis of resting-state fMRI. Front. Syst. Neurosci. 4, 13. [PubMed: 20577591]

Yang J, Gohel S, Zhang Z, Hatzoglou V, Holodny AI, Vachha BA, 2021. Glioma-induced disruption of resting-state functional connectivity and amplitude of low-frequency fluctuations in the

Author Manuscript Author Manuscript Author Manuscript Author Manuscript

salience network. American Journal of Neuroradiology 42 (3), 551–558. doi:10.3174/ajnr.A6929. [PubMed: 33384293]

Young J, Neveu CL, Byrne JH, Aazhang B, 2021. Inferring functional connectivity through graphical directed information. J. Neural Eng. 18 (4), 046019. doi:10.1088/1741-2552.

Yu X, Glen D, Wang S, Dodd S, Hirano Y, Saad Z, Reynolds R, Silva AC, Koretsky AP, 2012. Direct imaging of macrovascular and microvascular contributions to BOLD fMRI in layers IV-V of the rat whisker-barrel cortex. Neuroimage 59, 1451–1460. [PubMed: 21851857]

Yuan R, Di X, Kim EH, Barik S, Rypma B, Biswal BB, 2013. Regional homogeneity of resting-state fMRI contributes to both neurovascular and task activation variations. Magn. Reson. Imaging 31, 1492–1500. [PubMed: 23969197]

Zang Y, Jiang T, Lu Y, He Y, Tian L, 2004. Regional homogeneity approach to fMRI data analysis. Neuroimage 22, 394–400. [PubMed: 15110032]

Zang YF, He Y, Zhu CZ, Cao QJ, Sui MQ, Liang M, Tian LX, Jiang TZ, Wang YF, 2007. Altered baseline brain activity in children with ADHD revealed by resting-state functional MRI. Brain Dev. 29, 83–91. [PubMed: 16919409]

Zang YF, Zuo XN, Milham M, Hallett M, 2015. Toward a meta-analytic synthesis of the resting-state fMRI literature for clinical populations. Biomed. Res. Int, 4352652015.

Zhang K, Huang D, Shah NJ, 2018a. Comparison of Resting-State Brain Activation Detected by BOLD, Blood Volume and Blood Flow. Front. Hum. Neurosci. 12, 443. [PubMed: 30467468]

Zou Q, Yuan B-K, Gu H, Liu D, Wang DJ, Gao J-H, Yang Y, Zang Y-F, 2015. Detecting static and dynamic differences between eyes-closed and eyes-open resting states using ASL and BOLD fMRI. PloS one 10 (3), e0121757. [PubMed: 25816237]

Zou Q, Wu CW, Stein EA, Zang Y, Yang Y, 2009. Static and dynamic characteristics of cerebral blood flow during the resting state. Neuroimage 48, 515–524. [PubMed: 19607928]

Zou QH, Zhu CZ, Yang Y, Zuo XN, Long XY, Cao QJ, Wang YF, Zang YF, 2008. An improved approach to detection of amplitude of low-frequency fluctuation (ALFF) for resting-state fMRI: fractional ALFF. J. Neurosci. Methods 172, 137–141. [PubMed: 18501969]

Zuo XN, Xu T, Jiang L, Yang Z, Cao XY, He Y, Zang YF, Castellanos FX, Milham MP, 2013. Toward reliable characterization of functional homogeneity in the human brain: preprocessing, scan duration, imaging resolution and computational space. Neuroimage 65, 374–386. [PubMed: 23085497]

Zuo XN, Di Martino A, Kelly C, Shehzad ZE, Gee DG, Klein DF, Castellanos FX, Biswal BB, Milham MP, 2010. The oscillating brain: complex and reliable. Neuroimage 49, 1432–1445. [PubMed: 19782143]

Author Manuscript Author Manuscript Author Manuscript Author Manuscript

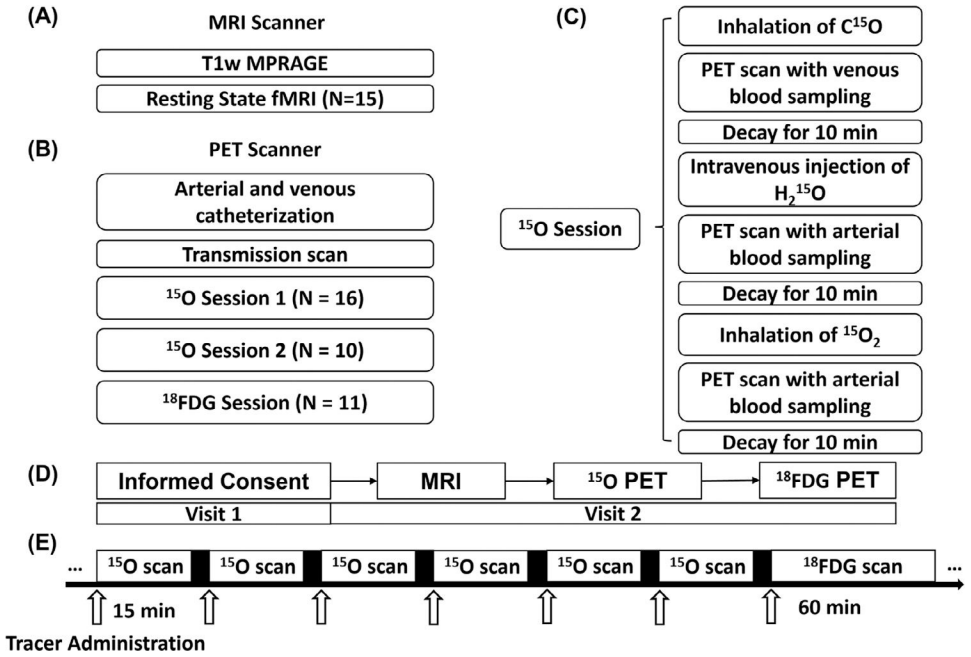

Fig. 1.

Illustration of data acquisition of the study.

Fig. 1A illustrates MRI procedures. Fig. 1B illustrates PET procedures. The PET ^{15}O session is further illustrated in 1C. The overall timeline of the experiment for each subject is illustraed in 1D. Timing of PET acquisition is illustrated in 1E. Arrows in 1E indicate bolus administrations of radiotracers, either through inhalation or intravenous injection.

Author Manuscript Author Manuscript Author Manuscript Author Manuscript

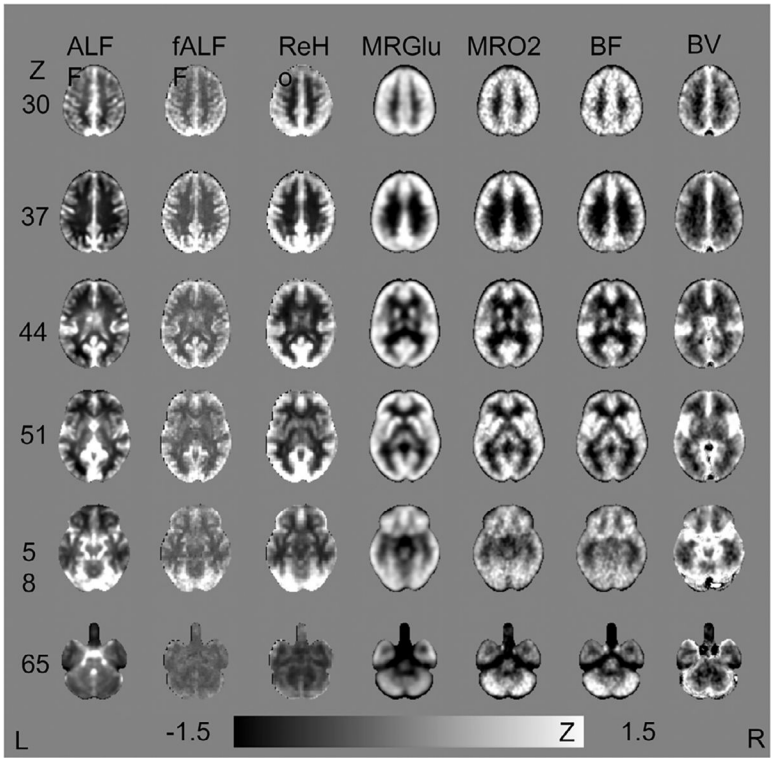

Fig. 2.

Spatial Similarities between ALFF, ReHo versus the PET Hemodynamic-metabolic Battery. Group-averaged images are spatially normalized to MNI 152 template (2mm isotropic resolution).Z-normalization are performed on normalized images within the gray matter and white matter mask. The scale of the color bar is −1.5 to 1.5.

Author Manuscript Author Manuscript Author Manuscript Author Manuscript

Fig. 3.

Regions Showing Different Regional Contrast in the Voxel-wise BOLD-PET Paired Comparisons.

Maps from individual subjects in each modality are z-normalized as Fig. 2, maintaining regional contrast, and compared pair-wise, resulting in voxel-wise p maps. Scale of the color bar before negative log transform is (0.0001, 0.01). Regions of gray color do not have significantly different values (z-normalized), indicating the spatial contrast are not significantly different.

Author Manuscript Author Manuscript Author Manuscript Author Manuscript

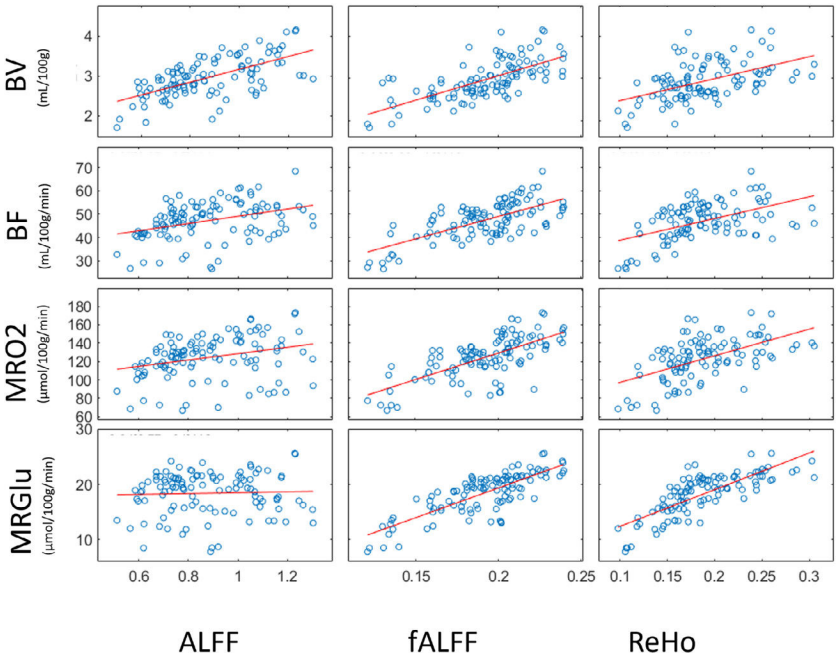

Fig. 4.

Linear Regression of BOLD Indices (ALFF, fALFF and ReHo) and PET Hemodynamic-metabolic Battery (BV, BF, MRO_2 and MRGlu).

Blue dots indicate mean values acquired with gray matter AAL region as ROIs on group-averaged images. Resulting correlation coefficient are reported in the Supplementary Results 1.2 Table A.

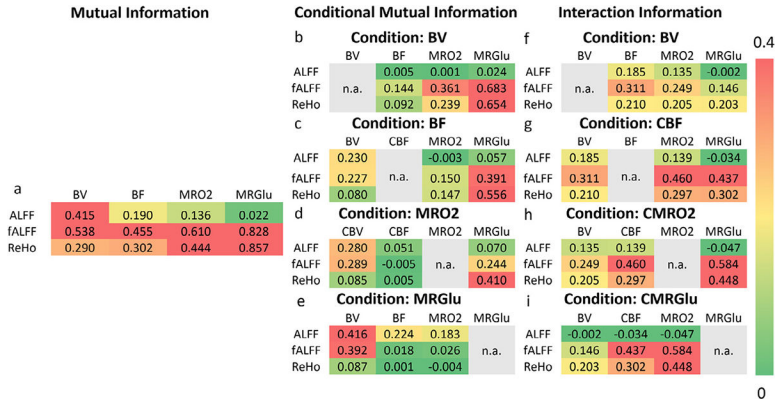

Fig. 5.

Conditional Mutual Information and Interaction Information Analyses of BOLD Metrics and PET Hemodynamic-metabolic Battery. Conditional MI for ALFF, fALFF and ReHo are presented in separated tables. The mutual information in each pair of comparison, after statistically removing the effect of a certain condition. Scale of the color bar is 0–0.4. In the conditional mutual information analyses, the metrics that being used as a condition will not be computed with a conditional mutual information and interaction information, which is listed as “n.a.” (not available) in gray color.

Author Manuscript Author Manuscript Author Manuscript Author Manuscript

Author Manuscript Author Manuscript Author Manuscript Author Manuscript

Table 1

Voxel-wise cross correlation and region-wise linear correlation among BOLD and PET metrics.

	Group Averaged				Per-Subject			
(a)	Voxel-wise Cross Correlation			(c)	Voxel-wise Cross Correlation			
		ALFF	fALFF	ReHo		ALFF ±0.10	fALFF	ReHo
	MRGlu	−0.1	0.49	0.63	MRGlu	−0.05±0.06	0.29± 0.05	0.41±0.05
	MRO2	0.06	0.39	0.53	MRO2	0.02±0.05	0.16± 0.04	0.24±0.05
	BF	0.15	0.36	0.49	BF	0.07±0.06	0.15± 0.04	0.23±0.05
	BV	0.29	0.31	0.37	BV	0.18±0.07	0.14± 0.06	0.18±0.08
(b)	Across-region Linear Correlation				(d)	Across-region Linear Correlation		
		ALFF	fALFF	ReHo		ALFF	fALFF	ReHo
	MRGlu	0.04	0.79 *	0.78 *	MRGlu	−0.42±0.12	0.49±0.17	0.60 ±0.10 *
	MRO2	0.29	0.68 *	0.54 *	MRO2	−0.08±0.15	0.22±0.09	0.29 ±0.12
	BF	0.37 *	0.68 *	0.50 *	BF	−0.02± 0.21	0.12±0.11	0.20 ±0.11
	BV	0.64 *	0.68 *	0.50 *	BV	0.27±0.12	0.05±0.17	−0.03±0.10

Table 1 (a) and (b): Spatial similarity and value correspondence on group-averaged images. Table 1 (c) and (d): Spatial similarity and value correspondence on per-subject images (mean and standard deviation). Voxel-wise cross correlation, compute by fslcc, does not output a p value. Voxel-wise cross correlation is performed on original images, to quantify spatial similarity.

* $P < 0.0001$